Isolation and measurement of GIPR mRNA. Total RNA was extracted from tissues (pancreatic islets, proximal jejunum, and adipose tissues) of C57/BL6 mice and Wistar rats (Shimizu) and mouse pancreatic β-cell line MIN6 cells with RNeasy mini kit (Qiagen, Valencia, CA). Islets were isolated by collagenase digestion (29). The extracted RNA was treated with DNase (Qiagen), and the cDNA was prepared by reverse transcription (Superscript II; Invitrogen, Grand Island, NY) with an oligo(dT) primer. To detect mouse full-length GIPR, COOH-terminal and NH_2-terminal primers of GIPR were designed as follows: forward, 5′-CTTTTCAAGGATGCCCCTGCGGTTGC-3′; reverse, 5′-CCTTTACCTAGCAGTAACTTTTCCAAGA-3′. The cDNA was amplified through 35 cycles with denaturation at 96°C for 15 s, annealing at 60°C for 30 s, and extension at 72°C for 2 min. To clearly detect splice variants of GIPR, a pair of GIPR primers was designed as follows: mouse GIPR forward, 5′-CTGCCTGCCGCACGGCCCAGAT-3′; reverse, 5′-CAAATGGCTTTGACTTCGTTG-3′; rat GIPR forward, 5′-CTGCCTGCCGCACAGCCCAGAT-3′; reverse, 5′- CAAATGGCTTTGACTTCGTTG -3′. The cDNA was amplified through 40 cycles with denaturation at 95°C for 15 s, annealing at 55°C for 15 s, and extension at 72°C for 30 s. The PCR products were fractioned on 2% agarose gels. Negative controls of cDNAs of tissues were prepared in the absence of reverse transcriptase at the reverse transcription step.

GIPR mRNA levels in the islets were measured by quantitative RT-PCR using ABI PRISM 7000 Sequence Detection System (Applied Biosystems, Foster City, CA). The mouse sequences of forward and reverse primers to evaluate total GIPR expression were 5′-CCTCCACTGGGTCCCTACAC-3′ and 5′-GATAAACACCCTCCACCAGTAG-3′, respectively, whereas the sequences of forward and reverse primers to evaluate truncated GIPR expression were 5′-CCTACCCCGTGGAACCAG-3′ and 5′-GTGGTGGGGAGCCAAGAT-3′, respectively. SYBR Green PCR Master Mix (Applied Biosystems) was prepared for PCR run. The thermal cycling conditions were denaturation at 95°C for 10 min followed by 50 cycles at 95°C for 15 s and 60°C for 1 min. Total GIPR mRNA levels were corrected for GAPDH (Applied Biosystems) mRNA levels.

Plasmid construction. The cDNA fragments of mouse wild-type GIPR, truncated GIPR, and $G_s\alpha$ protein were obtained from mouse (C57BL/6) islets by RT-PCR. The cDNA fragment of wild-type GIPR was cloned into pCMV-6c vector and pFLAG-CMV-5b vector (wild-type GIPR-FLAG; Sigma, St. Louis, MO). The cDNA fragment of truncated GIPR was cloned into pCMV-6c vector and pAcGFP-N1 vector (truncated GIPR-GFP; Takara, Tokyo, Japan). The two GIPR constructs were FLAG- or green fluorescent protein (GFP)-tagged at the COOH terminus. The cDNA fragment of mouse $G_s\alpha$ protein was cloned into pCMV-6c vector.

Cell culture and transfection. COS-7 cells were seeded in 10-cm dishes and cultured in Dulbecco's modified Eagle's medium supplemented with 10% fetal bovine serum. Expression plasmids of wild-type GIPR, truncated GIPR, wild-type GIPR-FLAG, and truncated GIPR-GFP were transfected into COS-7 cells using FuGENE 6 transfection reagent (Roche, Basel, Switzerland). Plasmid (5 μg/well) was diluted into serum-free medium, and FuGENE 6 reagent was added and incubated at room temperature for 30 min. After incubation, the mixture was added to COS-7 cells.

Measurement of intracellular cAMP level in GIPR-expressing COS-7 cells. COS-7 cells were transfected with the wild-type GIPR expression plasmid and the truncated GIPR expression plasmid using the amounts indicated in figure legends, passaged after 24 h into 12-well plates (1×10^5 cells/well), and cultured for an additional 48 h. The cells were washed twice with phosphate-buffered saline (PBS), and the reaction was started in 0.5 ml of Krebs-Ringer bicarbonate buffer (KRBB) containing 0.1 mM 3-isobutyl-1-methylxanthine (IBMX) with various concentrations of mouse GIP (provided by Sanwakagaku Kenkyusho, Mie, Japan) and then incubated at 37°C for 30 min. Incubation buffers were removed and the cells lysed by addition of 0.1 M HCl (0.5 ml/well) to each well (15). Plates were incubated at room temperature for 15 min with gentle rotation. The samples were centrifuged for 10 min at 600 *g*. cAMP levels were measured by enzyme immunoassay (cAMP low pH EIA kit; R&D Systems, Minneapolis, MN). Data were expressed as the increment with GIP treatment from basal cAMP levels.

Fluorescence microscopy. Immunofluorescence staining was performed using COS-7 cells either transfected with the wild-type GIPR-FLAG expression plasmid (2 μg) or the truncated GIPR-GFP expression plasmid (2 μg) or cotransfected with the two plasmids (1 μg each) with $G_s\alpha$ protein expression plasmid (2 μg). We used $G_s\alpha$ protein expression plasmid for structural stability of wild-type GIPR on plasma membrane (11). The cells were cultured on coverslips for 72 h, washed twice with PBS, and treated with acetone-methanol (1:1) for 4 min. After being washed sequentially with PBS containing 1% bovine serum albumin (BSA), the cells were incubated at room temperature for 24 h with anti-GFP monoclonal mouse antibody (Sigma) and anti-FLAG polyclonal rabbit antibody (Sigma) or anti-calnexin rabbit polyclonal antibody (Stressgen, San Diego, CA) in PBS containing 1% BSA. After being washed three times with PBS, the cells were immunostained at room temperature for 1 h using Cy3-conjugated anti-rabbit IgG (Sigma) or Alexa fluor 488 anti-mouse IgG (Molecular Probes, Eugene, OR) (23). Fluorescent images were analyzed using a confocal laser microscope LSM510 Meta (Carl Zeiss, Heidelberg, Germany).

Binding assay. Binding assay was performed using COS-7 cells either transfected with the wild-type GIPR expression plasmid (1 μg) or the truncated GIPR expression plasmid (1 μg) or cotransfected with the two plasmids (1 μg each) (total amount of plasmid DNA used for transfection was adjusted to 5 μg by adding pCMV-6c vector). After 72 h of incubation the cells were washed twice with PBS, and the collected cells were incubated with ^{125}I-labeled GIP (50,000 counts/min; Amersham Biosciences, Piscataway, NJ) in 1 ml of buffer containing 50 mM Tris (pH 7.4), 0.2 mM sucrose, 5 mM $MgCl_2$, and 1 mg/ml baeitracin at 22°C for 1 h in the absence or presence of 10^{-6} M nonradioactive GIP. Samples were filtered through Whatman GF/C filters (24 mm) and rapidly washed three times with ice-cold PBS. The radioactivity of the filters was measured in a γ-counter (22). Competitive binding assay was also performed using COS-7 cells transfected with the wild-type GIPR expression plasmid (1 μg) or cotransfected with the two plasmids (1 μg each). Various concentrations of nonradioactive GIP, ranging from 10^{-12} to 10^{-6} M, were used as competitors. Specific binding of radioactive GIP was calculated by subtracting binding of radioactive GIP in the presence of nonradioactive GIP. Protein content was measured by Bradford method. Data were expressed as specific binding to each of the GIPR-expressing cells after subtraction of the specific binding to cells transfected with pCMV-6c vector.

Immunoprecipitation and Western blot analysis. We performed Western blot analysis using COS-7 cells either transfected with the wild-type GIPR-FLAG expression plasmid (2 μg) or the truncated GIPR-GFP expression plasmid (2 μg) or cotransfected with the two plasmids (1 μg each). After 72 h of incubation, the collected cells were washed twice with PBS containing protease inhibitor (Complete; Roche) and suspended in 1 ml of PBS containing protease inhibitor. The cells were homogenized and centrifuged at 800 *g* for 5 min. The supernatant was centrifuged at 10,000 *g* for 10 min. The supernatant was further centrifuged at 100,000 *g* for 30 min to separate the endoplasmic reticulum (ER)-enriched fraction and the supernatant. The ER-enriched fraction was solubilized in 1 ml of PBS containing protease inhibitor and 2% Triton X-100 on ice for 15 min and centrifuged at 15,000 *g* for 10 min. The supernatant was incubated at 4°C for 2 h with mixing for immunoprecipitation using anti-FLAG M2 affinity beads (Sigma). The beads collected by centrifugation were washed three times with 1 ml PBS containing protease inhibitor, suspended in 20 μl of sample buffer (0.2 M Tris, 10% sucrose, 10% SDS, and 5 mM EDTA), and incubated at 98°C for 5 min. After centrifugation, the supernatants were electrophoresed through 5–16%

polyacrylamide gradient gels. The gels were subjected to immunoblotting using anti-FLAG polyclonal rabbit antibody (Sigma) or anti-GFP polyclonal rabbit antibody (Sigma) and anti-rabbit or anti-mouse IgG horseradish peroxdase-linked antibody (Amersham Biosciences). The immunoblots were visualized by electrochemiluminescence (Amersham Biosciences).

To determine whether the two GIPRs insert into the ER membrane, the ER-enriched fraction of COS-7 cells cotransfected with the two plasmids (1 μg each) were incubated in PBS containing 0.2 M sucrose in the absence or presence of 0.1 M Na_2CO_3 (pH 10.5) for 1 h on ice. After centrifugation at 100,000 *g* for 30 min, Western blot was performed with the supernatant and pellet using an antibody against FLAG or GFP.

Measurement of insulin secretion and intracellular cAMP production in isolated islets. Islets were isolated from mice and handpicked under a microscope. For insulin secretion studies, groups of 10 islets were preincubated at 37°C for 30 min in KRBB containing 2.8 mM glucose and 0.2% BSA and gassed with 95% O_2 and 5% CO_2. The islets were incubated at 37°C for 30 min in 0.5 ml of KRBB containing 2.8 mM or 11.1 mM glucose and 0.2% BSA in the absence or presence of high potassium (30 mM KCl). The islets were also incubated at 37°C for 30 min in 0.5 ml of KRBB containing 11.1 mM glucose and 0.2% BSA with or without mouse GIP (10^{-9} or 10^{-7} M) or 5 μM forskolin. Aliquots of the sample buffer were subjected to RIA assay for insulin. To determine insulin content, the islets were homogenized in 0.4 ml acid-ethanol and extracted at 4°C overnight. The acidic extracts were dried and subjected to insulin measurement.

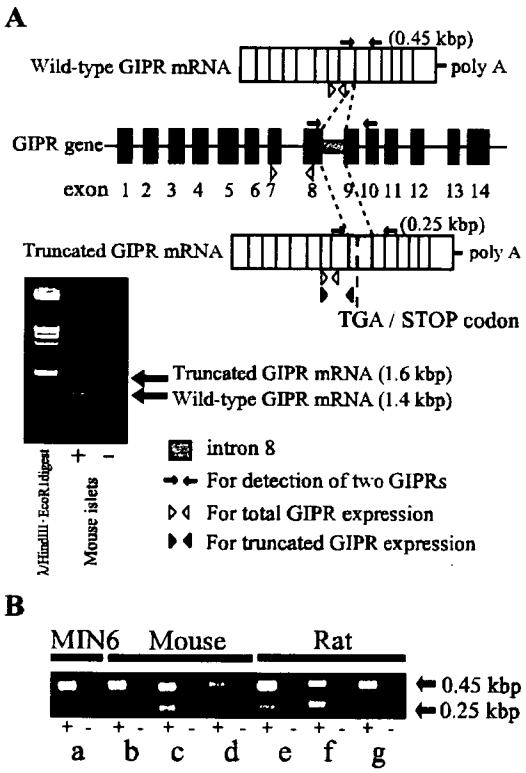

Fig. 1. Structure and expression of the splice variant gastric inhibitory polypeptide (GIP) receptor (GIPR). *A*: the structure of 2 splice variant GIPRs. PCR amplification of mouse (C57BL/6) islet cDNA was performed using COOH-terminal and NH_2-terminal primers of GIPR. The upper band (1.6 kbp) encodes a truncated GIPR isoform that retained the sequence of intron 8 (0.2 kbp) during RNA processing. The lower band (1.4 kbp) encodes wild-type GIPR isoform (full-length GIPR). A minus lane is negative control of mouse islet. The specific primer pair was designed to clearly detect 2 bands of GIPR by RT-PCR (arrows). The primer pair for quantitative RT-PCR to analyze total GIPR expression and truncated GIPR expression is indicated as open arrowhead and filled arrowhead, respectively. Intron 8 is indicated as gray box. *B*: tissue distribution of truncated GIPR in mice, rats, and MIN6 cells. The 0.25-kbp band shows the amplified DNA fragment of wild-type GIPR; the 0.45-kbp band shows that of truncated GIPR. cDNA was prepared from mouse (*a–d*) and rat (*e–f*) tissues, and RT-PCR was performed (*a*, MIN6 cells; *b* and *e*, adipose tissue; *c* and *f*, islets; *d* and *g*, proximal jejunum). A minus lane is negative control of each tissue.

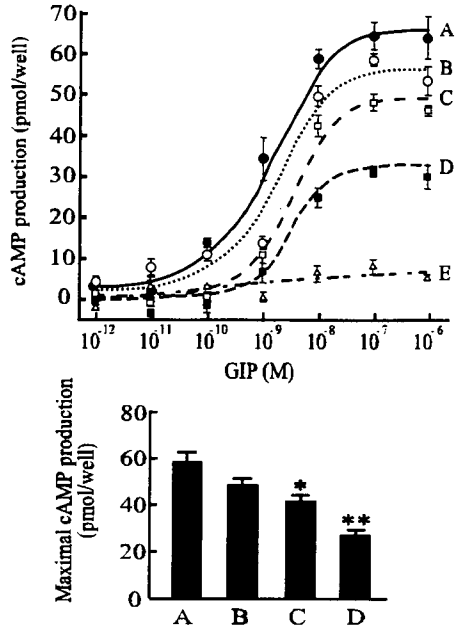

Fig. 2. Dose response analysis of GIP-induced cAMP production in GIPR-expressing COS-7 cells. *Top*: the ratios of the 2 GIPRs were as follows: wild-type GIPR expression plasmid DNA (μg) to truncated GIPR expression plasmid DNA (μg) = 1:0 (●; *A*), 1:0.5 (○; *B*), 1:1 (■; *C*), 1:2 (□; *D*), and 0:1 (△; E). The total amount of plasmid DNA used for each transfection was adjusted to 5 μg by adding pCMV-6c vector. Values are means ± SE. *Bottom*: cAMP induced by 10^{-6} M GIP is shown (n = 3–4). All ED_{50} values of GIP response curves were ~3.0 nM. Values are means ± SE. *$P < 0.05$; **$P < 0.01$ vs. cAMP induction of wild-type GIPR expression.

For cAMP production studies, 20 preincubated islets were incubated at 37°C for 30 min in 0.3 ml of KRBB containing 11.1 mM glucose, 0.2% BSA, 1 mM IBMX, and 10 mM HEPES (pH 7.4) with or without 10^{-9} M GIP, 10^{-7} M GIP, or 5 μM forskolin. The incubation was stopped by the addition of 60 μl of 2 M $HClO_4$. The samples were immediately mixed and sonicated in ice-cold water for 4 min. The samples were centrifuged for 4 min at 3,000 *g*, and aliquots (240 μl) were neutralized by 60 μl of 1 M Na_2CO_3 and diluted with 60 μl of 2 M HEPES (pH 7.4). cAMP levels were measured by EIA assay.

Statistical analysis. Values are expressed as means ± SE. Statistical analyses were performed using ANOVA and unpaired student's *t*-test. *P* values <0.05 were considered significant.

RESULTS

Identification of truncated GIPR. PCR amplification and sequencing of full-length GIPR from mouse islet cDNA revealed expression of two isoforms (Fig. 1*A*). The upper band (1.6 kbp) is characterized by unsplicing of intron 8 (0.2 kbp). As a result of the addition, the predicted amino acid reading frame is shifted within the region encoding transmembrane domain 4 and an in-frame stop codon is produced, generating a COOH-terminal truncated form of 263 amino acids desig-

nated as truncated GIPR. The lower band (1.4 kbp) corresponds to full-length GIPR of 460 amino acids designated as wild-type GIPR. To estimate truncated GIPR expression in different tissues, RT-PCR was performed using a different detection primer pair (Fig. 1*B*). Truncated GIPR was expressed not only in mouse islets but also in mouse proximal jejunum and adipose tissue. Truncated GIPR was also expressed in a mouse pancreatic β-cell line (MIN6), rat islets, proximal jejunum, and adipose tissue.

Function of truncated GIPR. To determine the functional properties of truncated GIPR, COS-7 cells were transfected with wild-type and truncated GIPR expression plasmid separately and stimulated with GIP (Fig. 2). In wild-type GIPR-expressing cells, GIP increased cAMP levels in a concentration-dependent manner. In contrast, GIP failed to stimulate cAMP induction in truncated GIPR-expressing cells. COS-7 cells were then cotransfected with wild-type and truncated GIPR expression plasmids. As the amount of truncated GIPR expression plasmid was increased from 0.5 to 2 μg in the presence of 1 μg of wild-type GIPR expression plasmid, maximal cAMP production induced by GIP was reduced, indicating that truncated GIPR had a dominant negative effect against wild-type GIPR. We examined whether truncated GIPR influenced glucagon-like peptide-1 (GLP-1)-induced cAMP production using GLP-1 receptor-expressing COS-7 cells. GLP-1-induced cAMP production was not decreased in the presence of truncated GIPR (data not shown), indicating that the dominant negative effect of truncated GIPR is specific to GIPR.

To determine how truncated GIPR affects wild-type GIPR in COS-7 cells, we constructed a COOH-terminal FLAG-tagged wild-type GIPR expression plasmid (wild-type GIPR-FLAG) and a COOH-terminal GFP-tagged truncated GIPR expression plasmid (truncated GIPR-GFP). When each of these expression plasmids was transfected into COS-7 cells (Fig. 3*A*, *a* and *b*), wild-type GIPR-FLAG was expressed on the cell surface

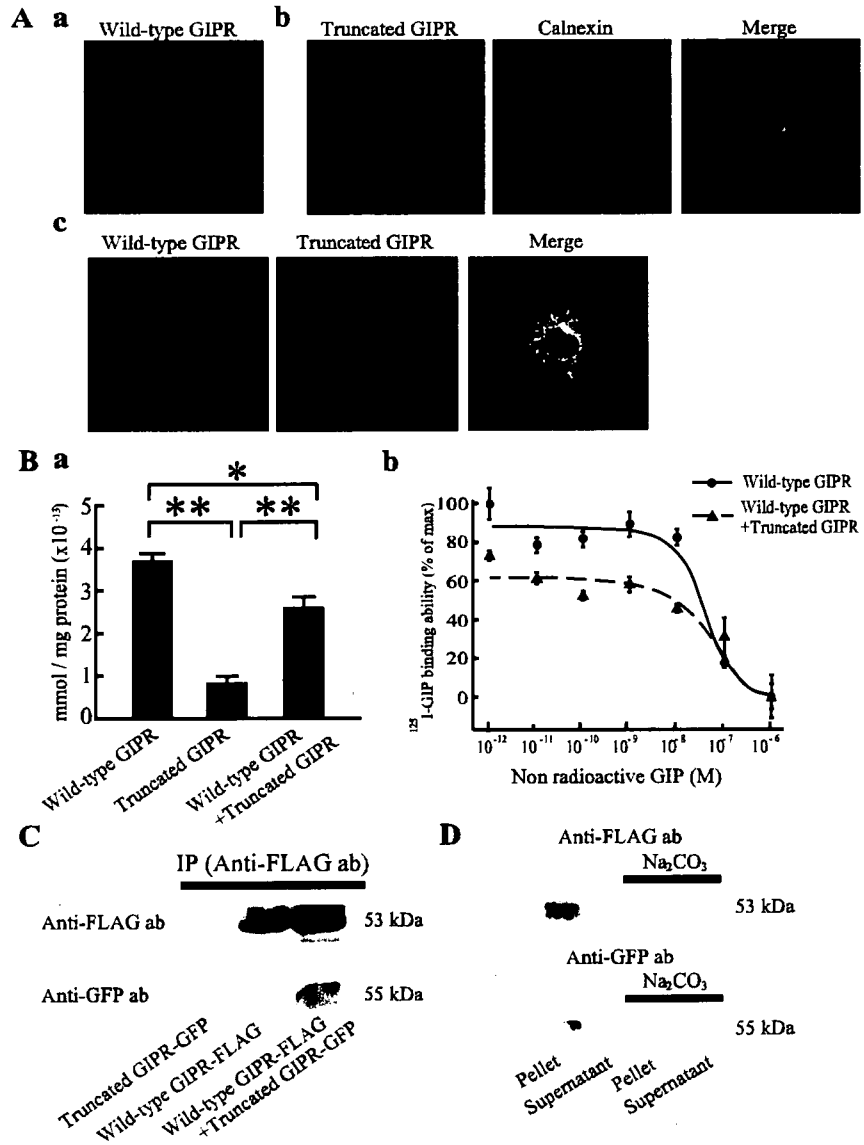

Fig. 3. Cellular localization and interaction of wild-type GIPR and truncated GIPR in GIPR-expressing COS-7 cells. *A*: immunofluorescence staining of the GIPR-expressing COS-7 cells. COS-7 cells were transfected with wild-type GIPR-FLAG (*a*) or truncated GIPR-green fluorescent protein (GFP) (*b*). To estimate localization of truncated GIPR-GFP, anti-calnexin antibody was used as endoplasmic reticulum (ER) maker (green, truncated GIPR-GFP; red, calnexin; yellow, merge). Cotransfection of the 2 GIPRs (*c*) was performed (red, wild-type GIPR-FLAG; green, truncated GIPR-GFP; yellow, merge). Localization of the GIPRs was analyzed by dual wavelength confocal microscopy. We repeated these experiments using 1×10^5 cells 3 times. *B*: binding assay analysis using GIPR-expressing COS-7 cells ($n = 4$; *a*). Competitive GIP binding curves using COS-7 cells transfected with wild-type GIPR (●) or cotransfected with two GIPRs (▲) (wild-type GIPR to truncated GIPR = 1:1 μg, $n = 5$; *b*). The IC_{50} values of binding curves were 5.6×10^{-8} and 7.2×10^{-8} M, respectively. Data are expressed as specific binding to each of the GIPR-expressing cells after subtraction of the specific binding to cells transfected with pCMV-6c vector. Values are means ± SE. $^*P < 0.05$; $^{**}P < 0.01$. *C*: immunoprecipitation and Western blot analysis of ER-enriched fractions of GIPR-expressing COS-7 cells. Immunoprecipitation was performed using anti-FLAG M2 affinity beads. Wild-type GIPR was detected in COS-7 cells transfected with wild-type GIPR alone and cotransfected with the 2 GIPRs using anti-FLAG polyclonal antibody. Truncated GIPR was detected only in COS-7 cells cotransfected with the 2 GIPRs using anti-GFP polyclonal antibody. *D*: Western blot analysis of ER-enriched fractions of the 2 GIPRs-expressing COS-7 cells with or without Na_2CO_3 treatment.

whereas truncated GIPR-GFP expression was limited to the ER, as resolved by anti-calnexin antibody. When both wild-type GIPR-FLAG and truncated GIPR-GFP were coexpressed in COS-7 cells (Fig. 3*A*, *c*), the expression of wild-type GIPR-FLAG on the cell surface decreased and remained highly within the ER. To determine whether the tags of the receptor influenced receptor trafficking, we constructed tag-changed plasmids [a COOH-terminal GFP-tagged wild-type GIPR expression plasmid (wild-type GIPR-GFP) and a COOH-terminal FLAG-tagged truncated GIPR expression plasmid (truncated GIPR-FLAG)] and transfected them into COS-7 cells. Truncated GIPR-FLAG also was located in the ER and decreased wild-type GIPR-GFP trafficking from the ER to the cell membrane (data not shown). We performed a GIP binding assay using COS-7 cells transfected with nontagged wild-type and truncated GIPR. The GIP binding ability of wild-type GIPR was significantly decreased in the presence of truncated GIPR (Fig. 3*B*, *a*). Analysis of GIP binding curves by performing a competitive binding assay showed similar IC_{50} values of both curves (Fig. 3*B*, *b*).

Immunoprecipitation was performed on the prepared ER-enriched fractions of COS-7 cells transfected with the two GIPRs to determine whether truncated GIPR interacts with wild-type GIPR (Fig. 3*C*). In the ER-enriched fraction of cotransfected cells, immunoreactive truncated GIPR-GFP could be detected after immunoprecipitation with the FLAG-tagged wild-type GIPR, indicating that truncated GIPR interacts with wild-type GIPR on the ER membrane. Western blot analysis was performed using the ER-enriched fraction treated by Na_2CO_3 to determine whether the two GIPRs are inserted into the ER membrane (Fig. 3*D*). With Na_2CO_3 treatment peripheral membrane proteins are solubilized into the buffer, whereas integral membrane proteins are insoluble. Two GIPRs were detected in the pellet of the ER-enriched fraction untreated by Na_2CO_3. The two GIPRs were also detected in the pellet of the ER-enriched fraction treated by Na_2CO_3, indicating that the two GIPRs are stably inserted into the ER membrane. Thus, truncated GIPR influenced trafficking of wild-type GIPR from the ER to the cell surface by interacting with wild-type GIPR in the ER.

GIPR sensitivity in islets of HFD mice. To analyze the functional significance of truncated GIPR in vivo, we investigated GIPR sensitivity of β-cells in obese mice induced by high-fat diet. Mice were fed high-fat chow or control fat chow for 10 wk. Body weight was significantly higher in HFD mice compared with CFD mice (37.9 ± 1.8 and 32.3 ± 0.83 g, respectively, $P < 0.05$). To determine the effect of high-fat diet on glucose homeostasis, we carried out OGTTs. Blood glucose levels were similar in HFD and CFD mice (Fig. 4*A*). We then measured plasma insulin levels at the indicated times during OGTTs. Plasma insulin levels were twofold higher in HFD mice at 15 min (1.4 ± 0.2 and 2.7 ± 0.3 ng/ml, respectively, $P < 0.05$), and the area under the curve of insulin secretion during OGTT was significantly increased in HFD mice compared with CHD mice (191.6 ± 21.2 and 130.8 ± 15.8 $ng \cdot ml^{-1} \cdot min^{-1}$, respectively, $P < 0.05$) (Fig. 4*B*). These results suggest compensatory hyperinsulinemia in an attempt to maintain blood glucose levels in high-fat diet-induced obese mice.

To determine sensitivity to GIP in the islets of HFD mice, GIP-induced insulin secretion from isolated islets of these mice

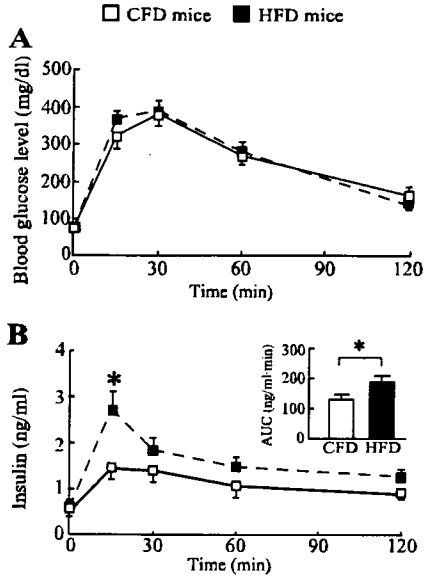

Fig. 4. Oral glucose tolerance tests (OGTTs) in control fat chow (CFD) and high-fat chow (HFD) mice. *A*: blood glucose levels during OGTTs in CFD (□) and HFD (■) mice ($n = 8$). *B*: plasma insulin levels during OGTTs in CFD (□) and HFD (■) mice ($n = 8$). Area under the curves of the insulin secretion during OGTTs in CFD mice (open bar) and HFD mice (filled bar) were also represented. Values are means ± SE. *$P < 0.05$ vs. CFD mice.

was examined in the presence of 11.1 mM glucose, in which incretin can potentiate insulin secretion. Insulin secretion stimulated by 11.1 mM glucose was similar in the islets of CHD and HFD mice (Fig. 5*A*). The islets of HFD mice showed significantly increased insulin secretion in response to 10^{-9} or 10^{-7} M GIP compared with those of CFD mice. On the other hand, forskolin, an adenylate-cyclase activator, increased insulin secretion in islets of CFD and HFD mice to a similar extent. In the presence of 2.8 and 11.1 mM glucose, insulin secretion stimulated by high potassium (30 mM) was also similar in the islets of CFD and HFD mice, respectively (Table. 1). The insulinotropic effect of GIP requires an increase in the level of intracellular cAMP in the β-cells, and cAMP production in the islets of HFD mice was significantly higher than that in CFD mice in the presence of GIP (Fig. 5*B*). However, forskolin increased intracellular cAMP production in the islets of CFD and HFD mice to a similar extent. Thus, GIPR sensitivity to GIP was increased specifically in the islets of HFD mice.

Expression of total and truncated GIPR in islets of HFD mice. To confirm differences in GIPR expression in islets between HFD and CFD mice, quantitative RT-PCR was performed. Total GIPR expression in the islets of HFD mice was similar to that of CFD mice (Fig. 6*A*). The relative expression level of truncated GIPR was then compared in the islets of HFD and CFD mice. The ratio of truncated GIPR to total GIPR expression in the islets of HFD mice was decreased by 32% compared with that in CFD mice (Fig. 6*B*).

DISCUSSION

In the present study, we have identified a novel splice variant GIPR expressed in mouse pancreatic β-cells and characterized its effect on GIPR sensitivity in high-fat diet-induced obese mice.

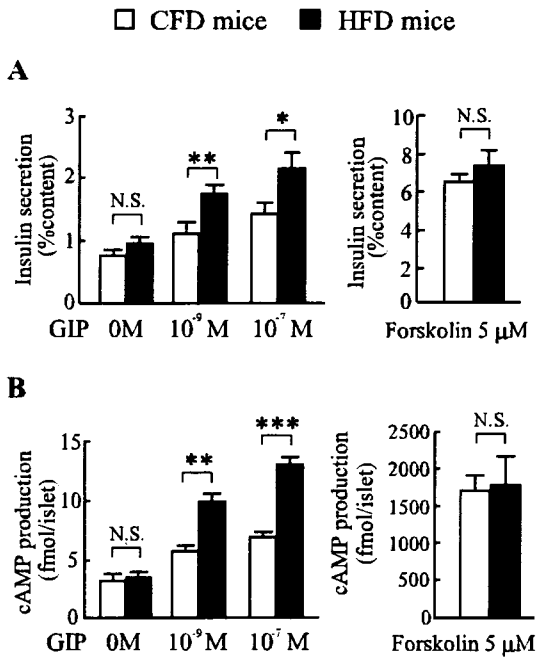

Fig. 5. Insulin secretion and cAMP production induced by GIP in isolated islets of CFD and HFD mice.Insulin secretion (n = 10; *A*) and intracellular cAMP levels (n = 6; *B*) in isolated islets of CFD (open bars) and HFD mice (filled bars) were examined in response to 10^{-9} or 10^{-7} M GIP in the presence of 11.1 mM glucose. The isolated islets of these mice were incubated with 5 μM forskolin to assess maximal insulin secretion and cAMP production. Values are means ± SE. $^{*}P < 0.05$, $^{**}P < 0.01$, and $^{***}P < 0.001$ vs. CFD mice.

We (21) previously investigated GIP-induced insulin secretion using *GIPR*$^{-/-}$ mice under high-fat feeding. The plasma insulin levels after meal ingestion were increased in high-fat diet-fed *GIPR*$^{+/-}$ mice compared with those in control diet-fed *GIPR*$^{+/+}$ mice, resulting in similar glucose levels. However, the postprandial glucose levels were increased by the lack of GIP-induced compensatory insulin secretion in high-fat diet-fed *GIPR*$^{-/-}$ mice, suggesting that increased insulin secretion due to enhanced GIP signaling is required to maintain glucose homeostasis in the obese state. In the present study, we have demonstrated hypersensitivity of GIPR to GIP in β-cells of high-fat-induced obese mice. Increased sensitivity of GIPR to GIP might result from increased expression of GIPR or hypersensitivity of intracellular GIP signal transduction. Some (9, 18) studies have reported that GIPR expression is an important factor in altering the GIP sensitivity of β-cells. In the study of diabetic Zucker fatty rats, GIPR mRNA expression and protein

Table 1. *Insulin secretion induced by glucose and high potassium (30 mM KCl) in the isolated islets of CFD and HFD mice*

%Content	CFD Mice	HFD Mice	*P* Value
2.8 mM glucose	0.69 ± 0.21	0.68 ± 0.07	NS
2.8 mM glucose + high potassium	0.99 ± 0.12	1.00 ± 0.17	NS
11.1 mM glucose	1.12 ± 0.14	1.22 ± 0.10	NS
11.1 mM glucose + high potassium	2.14 ± 0.25	2.42 ± 0.34	NS

Values are means ± SE; CFD (mice fed control fat chow; n = 5–6) vs. HFD mice (mice fed high-fat chow; n = 5–6). NS, not significant.

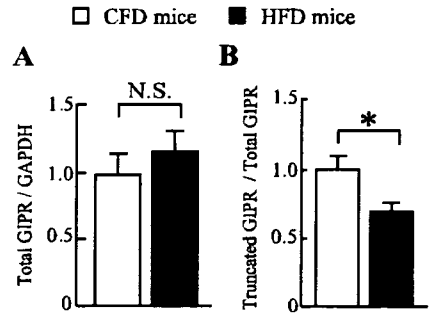

Fig. 6. Total and truncated GIPR expression in islets of CFD and HFD mice. Quantitative RT-PCR of total GIPR (*A*) and truncated GIPR (*B*) were assessed in islets of CFD (n = 6) and HFD mice (n = 6). The ratio of truncated GIPR to total GIPR (*B*) was calculated by quantitative RT-PCR of total GIPR and truncated GIPR. The data on HFD mice are shown relative to CFD mice. Values are means ± SE. $^{*}P < 0.05$ vs. CFD mice.

were decreased in islets compared with that of lean rats, which led to diminished GIPR sensitivity to GIP (17). Here, we found that total GIPR expression was not decreased and that GIPR sensitivity to GIP was increased in isolated islets of our HFD mice due to decreased expression of truncated GIPR, in contrast to the findings in diabetic obese rats. Our HFD mice were mild obese and mild hyperinsulinemia induced by high-fat feeding rather than by genetic factors. In addition, our obese mice did not have diabetes. Thus, differences of the expression of GIPR and subsequent GIPR sensitivity to GIP may be due to the different phenotypes of diabetic obese rats and HFD mice.

We had previously obtained the extra band of this GIPR variant as well as the band of wild-type GIPR when we amplified mouse islet cDNA to detect wild-type GIPR using NH_2-terminal and COOH-terminal primers of GIPR. We analyzed the cDNA sequence of the extra band and identified it as a splice variant of GIPR that was not produced by PCR error. Indeed, certain GIPR splice variants resulting in truncation have been reported in previous studies (7, 32). These splice variants were detected from cDNA libraries of human islets and insulinoma. However, the variants were not examined in regard to their regulatory role in GIPR sensitivity. In the present study, by evaluating the function of truncated GIPR in transfected COS-7 cells, we have shown that truncated GIPR has a dose-dependent dominant negative effect against wild-type GIPR.

GPCRs were generally thought to function as monomers, but recent studies (5, 12, 13) have reported that GPCRs can form homodimeric or heterodimeric complexes with receptors in the ER and that these complexes are important in receptor folding and trafficking to the plasma membrane. In the present study, we investigated the mechanism of negative action of truncated GIPR against wild-type GIPR function using immunochemistry and immunoprecipitation of cotransfected cells. Truncated GIPR interacted with wild-type GIPR in the ER and influenced wild-type receptor trafficking to the cell membrane. Some GPCRs have specific motifs for dimerization that are required for transport of the receptors from the ER to the cell surface (1, 8, 19, 26). Mutations in these motifs prevent dimerization with wild-type receptors and inhibit their trafficking to the cell membrane, indicating a dominant negative effect against the wild-type receptor (19, 26). Although these specific motifs are

not found in GIPR, truncated GIPR might have formed from complexes with wild-type GIPR in our experiments.

To evaluate the functional relevance of truncated GIPR in vivo, we investigated the expression of truncated GIPR in β-cells. The relative abundance of truncated GIPR expression was decreased in islets of HFD mice. The decreased dominant negative effect due to reduced expression of truncated GIPR might well be involved in augmented intracellular cAMP production and insulin secretion in response to GIP in islets in diet-induced obesity. Altered selective splicing in response to metabolic changes of the insulin receptor in β-cells was also reported (10), and hyperglycemia not only decreased total insulin receptor expression but also altered the relative expression ratio of the two insulin receptor isoforms in human islets, resulting in attenuation of insulin signal transduction. Although the mechanism of mRNA selective splicing of GIPR is unclear, insulin is reported (4) to influence the activity of the mRNA slicing regulator ASF/SF2, a serine/arginine-rich protein (SR protein). Further study is necessary to clarify the mechanism of GIPR mRNA selective splicing in response to metabolic changes.

In conclusion, we have identified a splice variant GIPR in mouse islets that has a dominant negative effect against the wild-type receptor by interacting in translocation of wild-type GIPR from the ER to the cell surface. Thus, reduced expression of truncated GIPR due to selective splicing and subsequent GIPR hypersensitivity to GIP may be involved in increased insulin secretion in response to GIP in metabolic states such as obesity.

ACKNOWLEDGMENTS

We thank K. Yamada and Dr. M. Sasaki for technical help.

GRANTS

This study was supported by Scientific Research Grants from the Ministry of Education, Culture, Sports, Science, and Technology (Japan); Health and Labor Sciences Research Grants for Comprehensive Research on Aging and Health from the Ministry of Health, Labor, and Welfare (Japan); and the 21st Century Center of Excellence Program (Japan).

REFERENCES

1. **Andersson H, D'Antona AM, Kendall DA, Von Heijne G, Chin CN.** Membrane assembly of the cannabinoid receptor 1: impact of a long N-terminal tail. *Mol Pharmacol* 64: 570–577, 2003.
2. **Boylan MO, Jepeal LI, Wolfe MM.** Structure of the rat glucose-dependent insulinotropic polypeptide receptor gene. *Peptides* 20: 219–228, 1999.
3. **Creuzfeldt W, Ebert R, Willms B, Frerichs H, Brown JC.** Gastric inhibitory polypeptide (GIP) and insulin in obesity: increased response to stimulation and defective feedback control of serum levels. *Diabetologia* 14: 15–24, 1983.
4. **Diamond RH, Du K, Lee VM, Mohn KL, Haber BA, Tewari DS, Taub R.** Novel delayed-early and highly insulin-induced growth response genes. Identification of HRS, a potential regulator of alternative pre-mRNA splicing. *J Biol Chem* 268: 15185–15192, 1993.
5. **Duvernay MT, Filipeanu CM, Wu G.** The regulatory mechanisms of export trafficking of G protein-coupled receptors. *Cell Signal* 17: 1457–1465, 2005.
6. **Flatt PR, Bailey CJ, Kwasowski P, Swanston-Flatt SK, Marks V.** Abnormalities of GIP in spontaneous syndromes of obesity and diabetes in mice. *Diabetes* 32: 433–435, 1983.
7. **Gremlich S, Porret A, Hani EH, Cherif D, Vionnet N, Froguel P, Thorens B.** Cloning, functional expression, and chromosomal localization of the human pancreatic islet glucose-dependent insulinotropic polypeptide receptor. *Diabetes* 44: 1202–1208, 1995.
8. **Hague C, Uberti MA, Chen Z, Hall RA, Minneman KP.** Cell surface expression of α_{1D}-adrenergic receptors is controlled by heterodimerization with α_{1B}-adrenergic receptors. *J Biol Chem* 279: 15541–15549, 2004.
9. **Holst JJ, Gromada J, Nauck MA.** The pathogenesis of NIDDM involves a defective expression of the GIP receptor. *Diabetologia* 40: 984–986, 1997.
10. **Hribal ML, Perego L, Lovari S, Andreozzi F, Menghini R, Perego C, Finzi G, Usellini L, Placidi C, Capella C, Guzzi V, Lauro D, Bertuzzi F, Davalli A, Pozza G, Pontiroli A, Federici M, Lauro R, Brunetti A, Folli F, Sesti G.** Chronic hyperglycemia impairs insulin secretion by affecting insulin receptor expression, splicing, and signaling in RIN beta cell line and human islets of Langerhans. *FASEB J* 17: 1340–1342, 2003.
11. **Ishihara T, Nakamura S, Kaziro Y, Takahashi T, Takahashi K, Nagata S.** Molecular cloning and expression of a cDNA encoding the secretin receptor. *EMBO J* 7: 1635–1641, 1991.
12. **Jones KA, Tamm JA, Craig DA, Durkin MM, Dai M, Yao WJ, Johnson M, Gunwaldsen C, Huang LY, Tang C, Shen Q, Salon JA, Morse K, Laz T, Smith KE, Nagarathnam D, Noble SA, Branchek TA, Gerald C.** GABA(B) receptors function as a heteromeric assembly of the subunits GABA(B)R1 and GABA(B)R2. *Nature* 396: 674–679, 1998.
13. **Jordan BA, Trapaidze N, Gomes I, Nivarthi R, Devi LA.** Oligomerization of opioid receptors with β_2-adrenergic receptors: a role in trafficking and mitogen-activated protein kinase activation. *Proc Natl Acad Sci USA* 98: 343–348, 2001.
14. **Kahn BB, Flier JS.** Obesity and insulin resistance. *J Clin Invest* 106: 473–481, 2000.
15. **Kubota A, Yamada Y, Hayami T, Yasuda K, Someya Y, Ihara Y, Kagimoto S, Watanabe R, Taminato T, Tsuda K, Seino Y.** Identification of two missense mutations in the GIP receptor gene: a functional study and association analysis with NIDDM: no evidence of association with Japanese NIDDM subjects. *Diabetes* 45: 1701–1705, 1996.
16. **Lemieux I, Pascot A, Couillard C, Lamarche B, Tchernof A, Almèras N, Bergeron J, Gaudet D, Tremblay G, Prud'homme D, Nadeau A, Després JP.** Hypertriglyceridemic waist: A marker of the atherogenic metabolic triad (hyperinsulinemia; hyperapolipoprotein B; small, dense LDL) in men? *Circulation* 102: 179–184, 2000.
17. **Lynn FC, Pamir N, Ng EH, McIntosh CH, Kieffer TJ, Pederson RA.** Defective glucose-dependent insulinotropic polypeptide receptor expression in diabetic fatty Zucker rats. *Diabetes* 50: 1004–1011, 2001.
18. **Lynn FC, Thompson SA, Pospisilik JA, Ehses JA, Hinke SA, Pamir N, McIntosh CH, Pederson RA.** A novel pathway for regulation of glucose-dependent insulinotropic polypeptide (GIP) receptor expression in beta cells. *FASEB J* 17: 91–93, 2003.
19. **Margeta-Mitrovic M, Jan YN, Jan LY.** Function of GB1 and GB2 subunits in G protein coupling of GABA(B) receptors. *Proc Natl Acad Sci USA* 98: 14649–14654, 2001.
20. **Miyawaki K, Yamada Y, Ban N, Ihara Y, Tsukiyama K, Zhou H, Fujimoto S, Oku A, Tsuda K, Toyokuni S, Hiai H, Mizunoya W, Fushiki T, Holst JJ, Makino M, Tashita A, Kobara Y, Tsubamoto Y, Jinnouchi T, Jomori T, Seino Y.** Inhibition of gastric inhibitory polypeptide signaling prevents obesity. *Nat Med* 8: 738–742, 2002.
21. **Miyawaki K, Yamada Y, Yano H, Niwa H, Ban N, Ihara Y, Kubota A, Fujimoto S, Kajikawa M, Kuroe A, Tsuda K, Hashimoto H, Yamashita T, Jomori T, Tashiro F, Miyazaki J, Seino Y.** Glucose intolerance caused by a defect in the entero-insular axis: a study in gastric inhibitory polypeptide receptor knockout mice. *Proc Natl Acad Sci USA* 96: 14843–14847, 1999.
22. **Mukai E, Ishida H, Kato S, Tsura Y, Fujimoto S, Takahashi A, Horie M, Tsuda K, Seino Y.** Metabolic inhibition impairs ATP-sensitive K^+ channel block by sulfonylurea in pancreatic β-cells. *Am J Physiol Endocrinol Metab* 274: E38–E44, 1998.
23. **Nakamura Y, Suzuki H, Sakaguchi M, Mihara K.** Targeting and assembly of mitochondrial translocase of outer membrane 22 (TOM22) into the TOM complex. *J Biol Chem* 279: 21223–21232, 2004.
24. **Pederson RA.** GIP. *Gut Peptides*, edited by Walsh J and Dockray G. New York: Raven, 1993, p. 217–259.
25. **Reaven GM.** Role of insulin resistance in human disease. *Diabetes* 37: 1066–1084, 1988.
26. **Salahpour A, Angers S, Mercier JF, Lagace M, Marullo S, Bouvier M.** Homodimerization of the β2-adrenergic receptor as a prerequisite for cell surface targeting. *J Biol Chem* 279: 33390–33397, 2004.
27. **Service FJ, Rizza RA, Westland RE, Hall LD, Gerich JE, Go VL.** Gastric inhibitory polypeptide in obesity and diabetes mellitus. *J Clin Endocrinol Metab* 58: 1133–1140, 1984.

28. **Stock S, Leichner P, Wong AC, Ghatei MA, Kieffer TJ, Bloom SR, Chanoine JP.** Ghrelin, peptide YY, glucose-dependent insulinotropic polypeptide, and hunger responses to a mixed meal in anorexic, obese, and control female adolescents. *J Clin Endocrinol Metab* 90: 2161–2168, 2005.
29. **Sutton R, Peters M, McShane P, Gray DW, Morris PJ.** Isolation of rat pancreatic islets by ductal injection of collagenase. *Transplantation* 42: 689–691, 1986.
30. **Tsukiyama K, Yamada Y, Yamada C, Harada N, Kawasaki Y, Ogura M, Bessho K, Li M, Amizuka N, Sato M, Udagawa N, Takahashi N, Tanaka K, Oiso Y, Seino Y.** Gastric inhibitory polypeptide as an endogenous factor promoting new bone formation following food ingestion. *Mol Endocrinol* 20: 1644–1651, 2006.
31. **Usdin TB, Mezey E, Button DC, Brownstein MJ, Bonner TI.** Gastric inhibitory polypeptide receptor, a member of the secretin-vasoactive intestinal peptide receptor family, is widely distributed in peripheral organs and the brain. *Endocrinology* 133: 2861–2870, 1993.
32. **Volz A, Göke R, Lankat-Buttgereit B, Fehmann HC, Bode HP, Goke B.** Molecular cloning, functional expression, and signal transduction of the GIP-receptor cloned from a human insulinoma. *FEBS Lett* 373: 23–29, 1995.
33. **Yamada Y, Hayami T, Nakamura K, Kaisaki PJ, Someya Y, Wang CZ, Seino S, Seino Y.** Human gastric inhibitory polypeptide receptor: cloning of the gene (GIPR) and cDNA. *Genomics* 29: 773–776, 1995.

Available online at www.sciencedirect.com
ScienceDirect
Metabolism Clinical and Experimental 57 (2008) 299 - 303
Metabolism
Clinical and Experimental
www.elsevier.com/locate/metabol

Factors responsible for age-related elevation in fasting plasma glucose: a cross-sectional study in Japanese men

Kentaro Toyoda[a], Mitsuo Fukushima[b,*], Rie Mitsui[a], Norio Harada[a], Hidehiko Suzuki[b], Tomomi Takeda[a], Ataru Taniguchi[c], Yoshikatsu Nakai[d], Toshiko Kawakita[e], Yuichiro Yamada[a], Nobuya Inagaki[a], Yutaka Seino[c]

[a]*Department of Diabetes and Clinical Nutrition, Graduate School of Medicine, Kyoto University, Kyoto 606-8507, Japan*
[b]*Health Informatics Research Group, Foundation for Biomedical Research and Innovation, Kobe, Hyogo 650-0047, Japan*
[c]*Division of Diabetes and Clinical Nutrition, Kansai-Denryoku Hospital, Osaka 553-0003, Japan*
[d]*Faculty of Medicine, School of Health Science, Kyoto University, Kyoto 606-8507, Japan*
[e]*Department of Internal Medicine, Kyoto Preventive Medical Center, Kyoto 604-8491, Japan*

Received 14 February 2006; accepted 15 October 2007

Abstract

To evaluate the factors associated with age-related increase in fasting plasma glucose (FPG) in Japanese men with normal fasting glucose, we measured FPG, fasting immunoreactive insulin, glycated hemoglobin, total cholesterol, triglyceride, and high-density lipoprotein cholesterol levels in health check examinees. Subjects with FPG less than 6.1 mmol/L together with glycated hemoglobin less than 5.6% were enrolled in the study. The homeostasis model assessment of insulin resistance (HOMA-IR) and HOMA-β were used as the indices of insulin sensitivity and insulin secretion, respectively. Fasting plasma glucose increased significantly with age ($r = 0.30$, $P < .0001$), and HOMA-β decreased significantly with age ($r = 0.24$, $P < .0001$). The HOMA-IR had no significant relation with age ($r = 0.06$, not significant), whereas body mass index and serum triglyceride were associated with HOMA-IR ($r = 0.49$, $P < .0001$ and $r = 0.33$, $P < .0001$, respectively). Thus, in Japanese male subjects with normal fasting glucose, it is suggested that the FPG increment with age is associated with decreased β-cell function rather than with insulin resistance. Further analyses were performed by comparing 3 groups: low FPG (FPG <5.0 mmol/L), high FPG (5.0 ≤ FPG < 5.6 mmol/L), and mild impairment of fasting glycemia (mild IFG) (5.6 ≤ FPG < 6.1 mmol/L). The insulin levels in mild IFG and high FPG were significantly higher than in low FPG ($P < .001$), but those in mild IFG were similar to those in high FPG. Analysis of the 3 subgroups revealed that, whereas insulin sensitivity was impaired more in high FPG, there was little compensatory increase in insulin in mild IFG, suggesting that β-cell function is already deteriorated when the FPG level is greater than 5.6 mmol/L.

1. Introduction

Type 2 diabetes mellitus is characterized by both decreasing insulin secretion and insulin sensitivity, partly due to genetic factors [1-3]. Although diabetes is a worldwide health problem [4], it is clear that there are ethnic differences in the pathophysiology of the decreasing glucose tolerance characteristic of its development [5]. Factors responsible for glucose intolerance occur from a prediabetic state: impaired glucose regulation according to the World Health Organization classification. Impaired glucose regulation comprises 2 subgroups: impaired fasting glycemia (IFG) characterized by increasingly impaired fasting plasma glucose (FPG) with 2-hour plasma glucose (2h-PG) within normal limits and impaired glucose tolerance (IGT) characterized by increasingly impaired 2h-PG [6,7]. We previously reported that insulin secretory capacity and insulin sensitivity are both decreased in Japanese subjects with IFG [8-10]. Although β-cell function and insulin sensitivity may well begin to deteriorate earlier, there are few studies of the normal glucose tolerance (NGT) population. Fasting plasma glucose is known to increase with age [11], and both insulin secretory capacity and insulin

* Corresponding author. Tel.: +81 78 304 5988; fax: +81 78 304 5989.
E-mail address: fukum@tri-kobe.org (M. Fukushima).

0026-0495/$ - see front matter © 2008 Elsevier Inc. All rights reserved.
doi:10.1016/j.metabol.2007.10.002

sensitivity are reported to decrease with age [12-14]. We have reported that some subgroups of Japanese NGT subjects show especially decreased β-cell function [15]. However, it is unclear whether deteriorated insulin secretion or insulin sensitivity is the primary factor in the increase in FPG during the period of development from NGT to IFG in Japanese.

In addition, the American Diabetes Association (ADA) lowered the cutoff value of IFG from 6.1 to 5.6 mmol/L [16]. Subjects with FPG from 5.6 to 6.1 mmol/L and with normal postprandial glucose level are categorized as having IFG in the ADA criteria, although they are categorized as having NGT in the criteria of the World Health Organization and the Japanese Diabetes Association. Thus, analysis of these subjects with mild IFG (mild impairment of fasting glucose) in view of insulin secretion and insulin sensitivity is crucial to elucidate the characteristic of subjects with borderline glucose dysregulation. To investigate the pathogenesis of prediabetes in Japanese, we compared insulin secretory capacity and insulin sensitivity in health check examinees exhibiting normal fasting glucose (NFG).

2. Subjects and methods

2.1. Subjects

Among health check examinees between 1993 and 2004 at Kyoto University Hospital, Kansai-Denryoku Hospital, and Kyoto Preventive Medical Center, 657 male subjects with FPG <6.1 mmol/L and glycated hemoglobin (HbA_{1c}) <5.6% were enrolled in the study (Table 1). Subjects with known history or signs of diabetes, previous gastrointestinal operation, liver disease, renal failure, endocrine disease, malignancy, hypertension, frequent heavy exercise, or history of medications before the study were excluded.

2.2. Measurements

Physical measurement (body height, body weight) and laboratory measurements (urine test, FPG, fasting immunoreactive insulin [F-IRI], HbA_{1c}, total cholesterol [TC], triglyceride [TG], and high-density lipoprotein cholesterol [HDL-C] level) were taken. The study was designed in compliance with the ethics regulations of the Helsinki Declaration. Blood samples were collected after overnight fasting for 16 hours [8]. Plasma glucose levels were measured by glucose oxidase method using the Hitachi Automatic Clinical Analyzer 7170 (Hitachi, Tokyo, Japan). Serum insulin levels were measured by radioimmunoassay (RIA beads II; Dainabot, Tokyo, Japan), which shows low cross-reaction with C-peptide of less than 0.005% and proinsulin less than 0.5% [8]. Glycated hemoglobin levels were measured by high-performance liquid chromatography methods. Serum TC, TG, and HDL-C levels were measured as reported previously [17]. To evaluate insulin resistance, we used the homeostasis model assessment of insulin resistance index (HOMA-IR) calculated by the formula FPG (in millimoles per liter) × IRI (in microunits per milliliter)/22.5. The HOMA-IR is a reliable measure of insulin resistance, correlating well with values obtained by glucose clamp and minimal model studies [18-20]. To calculate pancreatic β-cell function (HOMA β-cell), we used the formula 20 × IRI (in microunits per milliliter)/[FPG (in millimoles per liter) − 3.5] [18].

Table 1
Clinical characteristics of the subjects with NFG

	Data
n	657
Age (y)	44.9 ± 11.2
BMI (kg/m^2)	23.6 ± 2.8
HbA_{1c} (%)	4.8 ± 0.3
FPG (mmol/L)	5.1 ± 0.4
F-IRI (μU/mL)	5.2 ± 2.9
TC (mmol/L)	5.19 ± 0.88
TG (mmol/L)	1.45 ± 1.01
HDL-C (mmol/L)	1.45 ± 0.35

Data are mean ± SD.

2.3. Statistical analysis

Clinical data are expressed as mean ± SD. Analyses were performed using the STATVIEW 5 system (StatView, Berkeley, CA). Multiple regression analysis was used to compare age and FPG, HOMA-β, HOMA-IR, and body mass index (BMI). The same analysis was performed between HOMA-IR and BMI and TG. The NFG group was divided into low and high FPG and mild IFG, and the metabolic profiles were compared using analysis of variance. The data are expressed as mean ± SE. $P < .05$ is considered significant.

3. Results

3.1. Characteristics of the study population

As shown in Table 1, the mean age of the subjects is 44.9 ± 11.2 years and the mean BMI is 23.6 ± 2.8 kg/m^2. Among them, the number of subjects with BMI more than 30 are 22 (3.4%), concomitant with the representative epidemiologic studies in Japanese [21-23].

3.2. Correlation between age and FPG, HOMA-β, and HOMA-IR

Fig. 1A shows a positive relationship of FPG with age ($r = 0.30$, $P < .0001$; FPG [in millimoles per liter] = 0.011 × age + 4.6). Fig. 1B shows that HOMA-β has a negative correlation with age ($r = 0.24$, $P < .0001$), whereas there is no significant correlation between HOMA-IR and age ($r = 0.06$, not significant).

3.3. Correlation between HOMA-IR and BMI and serum TG levels

Fig. 2A, B shows that BMI and serum TG levels are associated with HOMA-IR ($r = 0.49$, $P < .0001$ and $r = 0.33$,

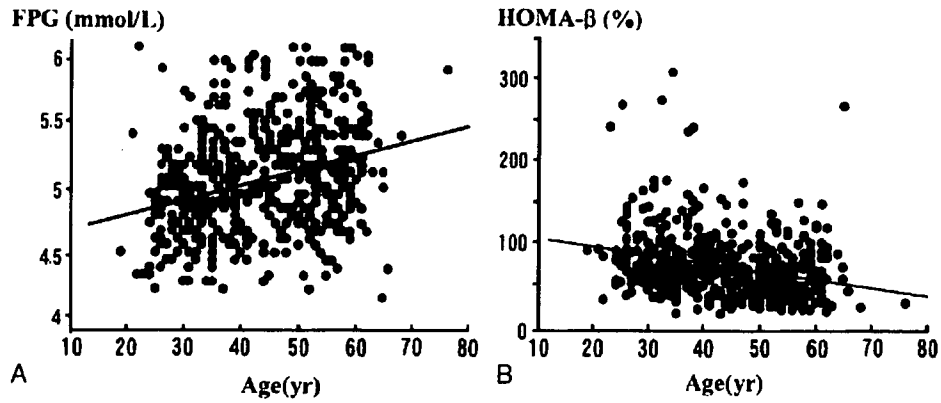

Fig. 1. Distribution of FPG (A) and HOMA-β (B) cell by age. The FPG increases with age ($r = 0.30$, $P < .0001$). The HOMA-β cell is negatively correlated with age ($r = 0.24$, $P < .0001$).

$P < .0001$, respectively). Multiple regression analysis shows that both BMI and TG are independently associated with HOMA-IR (standardized $\beta = 0.41$ and 0.15, respectively). Body mass index was the strongest determinant of HOMA-IR, and BMI did not increase with age significantly in Japanese men ($r = 0.07$, not significant).

3.4. Analysis of 3 subgroups of NFG subjects

To evaluate the factors involved in increasing FPG in Japanese NFG and the ADA recommendation of lowering the threshold of upper limit of normal FPG from 6.1 to 5.6 mmol/L [16], we divided our NFG subjects into 3 subgroups: low FPG (FPG <5.0 mmol/L), high FPG ($5.0 \leq$ FPG < 5.6 mmol/L), and mild impairment of fasting glucose (mild IFG) ($5.6 \leq$ FPG < 6.1 mmol/L); and age, BMI, TG, and insulin secretion and sensitivity were compared. As shown in Table 2, high FPG and mild IFG have higher age and BMI than low FPG (both $P < .0001$). Insulin in high FPG and mild IFG is increased compared with that in low FPG ($P < .001$); insulin in mild IFG is similar to that in high FPG. The HOMA-IR in high FPG and mild IFG is increased compared with that in low FPG ($P < .0001$). The HOMA-β in high FPG and mild IFG is decreased compared with that in low FPG ($P < .0001$); the HOMA-β in mild IFG is decreased compared with that in high FPG ($P < .001$).

4. Discussion

In this study, we analyzed the factors responsible for age-related elevation of FPG in Japanese men with NFG. Fasting plasma glucose was found to increase with age primarily because of reduced β-cell function rather than increased insulin resistance. In addition, we have elucidated that there was no compensatory increase in insulin secretion in mild IFG (FPG 5.6-6.1 mmol/L).

Our study subjects were composed only of men because the number of female subjects was 158, which is not comparable with male subjects. Some reports showed a difference between men and women in the elevation of FPG [24-26], and another showed similar results between men and women in the elevation of FPG [27]. We analyzed the results from our 158 female subjects, and we could not find

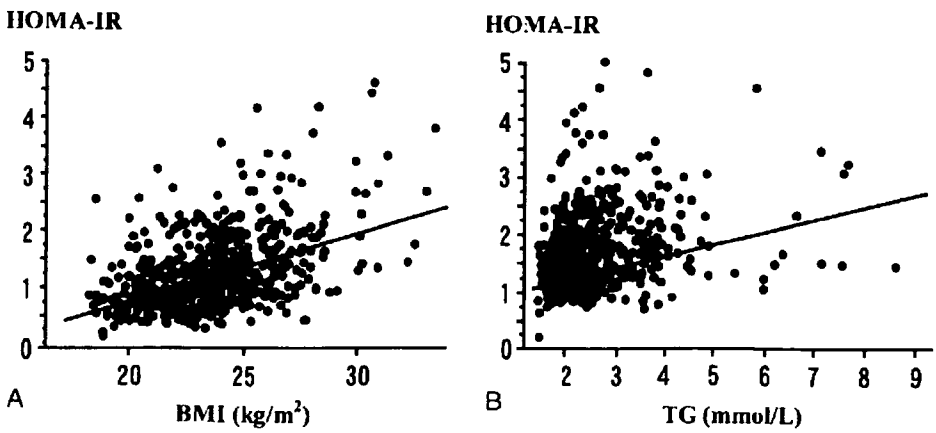

Fig. 2. Distribution of HOMA-IR by BMI (A) and TG (B). Both BMI and TG are associated with HOMA-IR (BMI: $r = 0.49$, $P < .0001$; TG: $r = 0.33$, $P < .0001$).

Table 2
Comparison of 3 FPG subgroups of NFG subjects

	Low FPG (FPG <5.0 mmol/L)	High FPG (5.0 ≤ FPG < 5.6 mmol/L)	Mild IFG (5.6 ≤ FPG < 6.1 mmol/L)
n	268	288	101
Age (y)	42.0 ± 0.7	45.7 ± 0.6[a]	49.8 ± 1.0[a,b]
BMI (kg/m^2)	23.0 ± 0.2	23.9 ± 0.1[a]	24.3 ± 0.3[a]
TC (mmol/L)	5.07 ± 0.05	5.23 ± 0.05[c]	5.35 ± 0.08[d]
TG (mmol/L)	1.30 ± 0.05	1.55 ± 0.06[d]	1.56 ± 0.09[c]
HDL-C (mmol/L)	1.45 ± 0.02	1.44 ± 0.02	1.45 ± 0.03
F-IRI (μU/mL)	4.6 ± 0.2	5.7 ± 0.2[a]	5.6 ± 0.3[c]
HOMA-IR	0.96 ± 0.04	1.31 ± 0.04[a]	1.44 ± 0.07[a]
HOMA-β (%)	78.5 ± 3.1	65.2 ± 1.9[a]	49.2 ± 2.4[a,b]

Data are mean ± SE.
[a] $P < .0001$ vs low FPG.
[b] $P < .001$ vs high FPG.
[c] $P < .05$ vs low FPG.
[d] $P < .005$ vs low FPG.
[e] $P < .0005$ vs low FPG.

remarkable differences with male subjects (data not shown). Further studies are necessary to elucidate the sex difference of the factors responsible for elevation of FPG. Although some reports showed an increase in insulin resistance in subjects older than 70 years, our male subjects were younger than 70 years. Insulin resistance in subjects older than 70 years was reported mainly because of the change in abdominal adiposity [28,29]; and in representative epidemiologic studies such as the Funagata study and the Hisayama study, the mean age of developing glucose intolerance is around 50 years in Japanese [21-23]. For these reasons, our subjects being around the age of 50 years was enough for our purpose in this study of elucidating the factors responsible for FPG elevation from normal to borderline glucose dysregulation.

Fasting plasma glucose increased by 0.011 mmol/L per year, in accord with previous reports [30]. The HOMA-β decreased by 0.85% per year, clearly indicating reduced basal insulin secretion. Although previous studies in whites and in other populations have found that insulin resistance is closely associated with age-related FPG elevation [12,31], HOMA-IR did not increase with age significantly in our subjects. To characterize the insulin resistance of our study population, we performed both simple and multiple regression analyses between HOMA-IR and the other measured factors. The BMI and serum TG levels were strongly associated with HOMA-IR ($P < .0001$), in accord with our previous results in Japanese diabetic patients [32]. Although BMI was the strongest determinant of HOMA-IR, it did not increase with age; the mean BMI of 23.6 kg/m^2 is in accord with Japanese statistical data [21-23] and is much lower than in whites [33,34]. The BMI of Asians in other studies is also reported to be lower, suggesting a common metabolic profile [35]. The leaner Japanese subjects in this study might therefore be expected to be less influenced by insulin resistance in comparison with whites.

Impaired fasting glycemia is a prediabetic state characterized by FPG elevation without increased 2h-PG. We previously reported that insulin secretory capacity and insulin sensitivity are both already decreased in IFG [8-10], suggesting the clinical importance of early deterioration of β-cell function and insulin sensitivity in developing prediabetes. In addition, we regarded the PG level of 5.6 mmol/L as an important FPG threshold value according to ADA recommendation [16]. Therefore, we compared insulin secretion and insulin sensitivity in 3 subgroups of NFG subjects: low FPG (FPG <5.0 mmol/L), high FPG (5.0 ≤ FPG < 5.6 mmol/L), and mild IFG (5.6 ≤ FPG < 6.1 mmol/L). Insulin secretion in mild IFG was not increased compared with that in high FPG, indicating impaired compensatory insulin secretion against increasing insulin resistance. Some reports have found that early-phase insulin secretion and insulin sensitivity are both decreased in NGT at a higher range of FPG (FPG >5.1-5.3 mmol/L) [36-38]. Fortunately, we could analyze 56 subjects during the 8-year follow-up period using oral glucose tolerance test results [39]. The subjects who developed from NFG to IFG showed decreasing insulin sensitivity and insulin secretory capacity, and those who developed from NFG to IGT showed decreased early insulin secretory response. These follow-up data were compatible with our previous data of IFG and IGT [5,8,10,39]. Taken together, these data indicate that insulin secretory capacity is already decreased in NGT at the higher range of FPG and that a lack of compensatory insulin secretion appears at greater than 5.6 mmol/L in FPG.

We find in Japanese NFG subjects that age-related FPG elevation is mainly due to decreased β-cell function rather than to increasing insulin resistance as in white subjects. In addition, analysis of 3 degrees of increasing FPG indicates that failure of compensatory insulin secretion is responsible for the elevation in FPG in these subjects. Thus, these data could be helpful in reconsideration of the threshold FPG for prediabetes to be recommended by the ADA [16]. However, decreasing the upper threshold of FPG entails increasing the IFG population, a costly social health problem [40]. Further studies are required to clarify the ethnic differences in the development of diabetes and diabetic complications and the value of clinical interventions in newly diagnosed IFG patients.

Acknowledgment

This study was supported in part by Health Sciences Research Grants for Comprehensive Research on Aging and Health; Research on Health Technology Assessment; and Research on Human Genome, Tissue Engineering, and Food Biotechnology from the Ministry of Health, Labour, and Welfare, and by Leading Project of Biostimulation from the Ministry of Education, Culture, Sports, Science, and Technology, Japan. We thank Use Techno, Ono Pharmaceutical, ABBOTT JAPAN, and Dainippon Pharmaceutical for their help in the study.

References

[1] Porte Jr D. Banting lecture 1990. Beta-cells in type II diabetes mellitus. Diabetes 1991;40:166-80.

[2] Lillioja S, Mott DM, Spraul M, et al. Insulin resistance and insulin secretory dysfunction as precursors of non–insulin-dependent diabetes mellitus. Prospective studies of Pima Indians. N Engl J Med 1993;329: 1988-92.

[3] DeFronzo RA. Lilly lecture 1987. The triumvirate: beta-cell, muscle, liver. A collusion responsible for NIDDM. Diabetes 1988;37:667-87.

[4] Mandavilli A, Cyranoski D. Asia's big problem. Nat Med 2004;10: 325-7.

[5] Fukushima M, Suzuki H, Seino Y. Insulin secretion capacity in the development from normal glucose tolerance to type 2 diabetes. Diabetes Res Clin Pract 2004;66:S37-43.

[6] Alberti KG, Zimmet PZ. Definition, diagnosis and classification of diabetes mellitus and its complications. Part 1: diagnosis and classification of diabetes mellitus provisional report of a WHO consultation. Diabet Med 1998;15:539-53.

[7] Suzuki H, Fukushima M, Usami M, et al. Factors responsible for development from normal glucose tolerance to isolated postchallenge hyperglycemia. Diabetes Care 2003;26:1211-5.

[8] Fukushima M, Usami M, Ikeda M, et al. Insulin secretion and insulin sensitivity at different stages of glucose tolerance: a cross-sectional study of Japanese type 2 diabetes. Metabolism 2004;53:831-5.

[9] Nishi Y, Fukushima M, Suzuki H, et al. Insulin secretion and insulin sensitivity in Japanese subjects with impaired fasting glucose and isolated fasting hyperglycemia. Diabetes Res Clin Pract 2005;70: 46-52.

[10] Izuka M, Fukushima M, Taniguchi A, et al. Factors responsible for glucose intolerance in Japanese subjects with impaired fasting glucose. Horm Metab Res 2007;39:41-5.

[11] Wiener K, Roberts NB. Age does not influence levels of HbA1c in normal subject. QJM 1999;92:169-73.

[12] Chang AM, Halter JB. Aging and insulin secretion. Am J Physiol Endocrinol Metab 2003;284:E7-E12.

[13] Paolisso G, Tagliamonte MR, Rizzo MR, et al. Advancing age and insulin resistance: new facts about an ancient history. Eur J Clin Invest 1999;29:758-69.

[14] Coon PJ, Rogus EM, Drinkwater D, et al. Role of body fat distribution in the decline in insulin sensitivity and glucose tolerance with age. J Clin Endocrinol Metab 1992;75:1125-32.

[15] Kuroe A, Fukushima M, Usami M, et al. Impaired beta-cell function and insulin sensitivity in Japanese subjects with normal glucose tolerance. Diabetes Res Clin Pract 2003;59:71-7.

[16] Report of the expert committee on the diagnosis and classification of diabetes mellitus. Diabetes Care 2003;26:S5-S20.

[17] Taniguchi A, Fukushima M, Sakai M, et al. Remnant-like particle cholesterol, triglycerides, and insulin resistance in nonobese Japanese type 2 diabetic patients. Diabetes Care 2000;23:1766-9.

[18] Bonora E, Targher G, Alberiche M, et al. Homeostasis model assessment closely mirrors the glucose clamp technique in the assessment of insulin sensitivity: studies in subjects with various degrees of glucose tolerance and insulin sensitivity. Diabetes Care 2000;23:57-63.

[19] Matthews DR, Hosker JP, Rudenski AS, et al. Homeostasis model assessment: insulin resistance and beta-cell function from fasting plasma glucose and insulin concentrations in man. Diabetologia 1985; 28:412-9.

[20] Fukushima M, Taniguchi A, Sakai M, et al. Homeostasis model assessment as a clinical index of insulin resistance. Comparison with the minimal model analysis. Diabetes Care 1999;22:1911-2.

[21] Ohmura T, Ueda K, Kiyohara Y, et al. The association of the insulin resistance syndrome with impaired glucose tolerance and NIDDM in the Japanese general population: the Hisayama study. Diabetologia 1994;37:897-904.

[22] Tominaga M, Eguchi H, Manaka H, et al. Impaired glucose tolerance is a risk factor for cardiovascular disease, but not impaired fasting glucose. The Funagata diabetes study. Diabetes Care 1999;22:920-4.

[23] Ministry of Health, Labour and Welfare Statistical database: Statistics and Information Department, second edition, chapter 1 "Public health"

[24] Williams JW, Zimmet PZ, Shaw JE, et al. Gender differences in the prevalence of impaired fasting glycaemia and impaired glucose tolerance in Mauritius. Does sex matter? Diabet Med 2003;20:915-20.

[25] Schianca GP, Castello L, Rapetti R, et al. Insulin sensitivity: gender-related differences in subjects with normal glucose tolerance. Nutr Metab Cardiovasc Dis 2006;16:339-44.

[26] Rutter MK, Parise H, Benjamin EJ, et al. Impact of glucose intolerance and insulin resistance on cardiac structure and function: sex-related differences in the Framingham Heart Study. Circulation 2003;107: 448-54.

[27] Yates AP, Laing I. Age-related increase in haemoglobin A1c and fasting plasma glucose is accompanied by a decrease in beta cell function without change in insulin sensitivity: evidence from a cross-sectional study of hospital personnel. Diabet Med 2002;19:254-8.

[28] DeNino WF, Tchernof A, Dionne IJ, et al. Contribution of abdominal adiposity to age-related differences in insulin sensitivity and plasma lipids in healthy nonobese women. Diabetes Care 2001;24:925-32.

[29] Bryhni B, Jenssen TG, Olafsen K, et al. Age or waist as determinant of insulin action? Metabolism 2003;52:850-7.

[30] Bando Y, Ushiogi Y, Okafuji K, et al. The relationship of fasting plasma glucose values and other variables to 2-h postload plasma glucose in Japanese subjects. Diabetes Care 2001;24:1156-60.

[31] Utzschneider KM, Carr DB, Hull RL, et al. Impact of intra-abdominal fat and age on insulin sensitivity and beta-cell function. Diabetes 2004; 53:2867-72.

[32] Taniguchi A, Fukushima M, Sakai M, et al. The role of the body mass index and triglyceride levels in identifying insulin-sensitive and insulin-resistant variants in Japanese non–insulin-dependent diabetic patients. Metabolism 2000;49:1001-5.

[33] Kuczmarski MF, Kuczmarski RJ, Najjar M. Effects of age on validity of self-reported height, weight, and body mass index: findings from the Third National Health and Nutrition Examination Survey, 1988-1994. J Am Diet Assoc 2001;101:28-34.

[34] Flegal KM, Carroll MD, Ogden CL, et al. Prevalence and trends in obesity among US adults, 1999-2000. JAMA 2002;288:1723-7.

[35] Qiao Q, Nakagami T, Tuomilehto J, et al. Comparison of the fasting and the 2-h glucose criteria for diabetes in different Asian cohorts. Diabetologia 2000;43:1470-5.

[36] Piche ME, Arcand-Bosse JF, Despres JP, et al. What is a normal glucose value? Differences in indexes of plasma glucose homeostasis in subjects with normal fasting glucose. Diabetes Care 2004;27:2470-7.

[37] Sato Y, Komatsu M, Katakura M, et al. Diminution of early insulin response to glucose in subjects with normal but minimally elevated fasting plasma glucose. Evidence for early beta-cell dysfunction. Diabet Med 2002;19:566-71.

[38] Godsland IF, Jeffs JA, Johnston DG. Loss of beta cell function as fasting glucose increases in the non-diabetic range. Diabetologia 2004; 47:1157-66.

[39] Mitsui R, Fukushima M, Nishi Y. Factors responsible for deteriorating glucose tolerance in newly diagnosed type 2 diabetes in Japanese men. Metabolism 2006;55:53-8.

[40] Genuth S, Alberti KG, Bennett P, et al. Follow-up report on the diagnosis of diabetes mellitus. Diabetes Care 2003;26:3160-7.

Available online at www.sciencedirect.com
ScienceDirect
Biochemical and Biophysical Research Communications 367 (2008) 793–798
BBRC
www.elsevier.com/locate/ybbrc

GLP-1 receptor signaling protects pancreatic beta cells in intraportal islet transplant by inhibiting apoptosis

Kentaro Toyoda [a], Teru Okitsu [b], Shunsuke Yamane [a], Taeko Uonaga [a], Xibao Liu [a], Norio Harada [a], Shinji Uemoto [c], Yutaka Seino [d], Nobuya Inagaki [a,e,*]

[a] *Department of Diabetes and Clinical Nutrition, Graduate School of Medicine, Kyoto University, 54 Kawahara-cho, Shogoin Sakyo-ku, Kyoto 606-8507, Japan*
[b] *Transplantation Unit, Kyoto University Hospital, Kyoto 606-8507, Japan*
[c] *Department of Surgery, Graduate School of Medicine, Kyoto University, Kyoto 606-8507, Japan*
[d] *Kansai Denryoku Hospital, Osaka 553-0003, Japan*
[e] *CREST of Japan Science and Technology Cooperation (JST), Kyoto, Japan*

Received 6 January 2008
Available online 22 January 2008

Abstract

To clarify the cytoprotective effect of glucagon-like peptide-1 receptor (GLP-1R) signaling in conditions of glucose toxicity *in vivo*, we performed murine isogenic islet transplantation with and without exendin-4 treatment. When a suboptimal number of islets (150) were transplanted into streptozotocin-induced diabetic mice, exendin-4 treatment contributed to the restoration of normoglycemia. When 50 islets expressing enhanced green fluorescent protein (EGFP) were transplanted, exendin-4 treatment reversed loss of both the number and mass of islet grafts one and 3 days after transplantation. TUNEL staining revealed that exendin-4 treatment reduced the number of apoptotic beta cells during the early posttransplant phase, indicating that GLP-1R signaling exerts its cytoprotective effect on pancreatic beta cells by inhibiting their apoptosis. This beneficial effect might be used both to ameliorate type 2 diabetes and to improve engraftment rates in clinical islet transplantation.

Keywords: Exendin-4; Glucagon-like peptide-1; Cytoprotection; Apoptosis; Enhanced green fluorescent protein; Islet transplantation; Islet engraftment

Glucagon-like peptide-1 (GLP-1) is a physiological incretin, an intestinal hormone released in response to nutrient ingestion that stimulates glucose-dependent insulin secretion [1,2]. Recent studies have demonstrated that GLP-1 has beneficial effects on pancreatic beta cells [3–6], one of which is inhibition of apoptosis of native beta cells. *In vitro* studies have shown that GLP-1 receptor (GLP-1R) signaling has various beneficial actions such as ameliorating ER stress [7,8] and oxidative stress [9]. However, demonstration of the *in vivo* cytoprotective effect in an animal model of type 2 diabetes (T2DM) is problematic because enhancement of GLP-1R signaling reduces blood glucose levels due to its insulinotropic action [4,5], glucagonostatic action on alpha cells [10], and improvement of insulin sensitivity [11], which makes it difficult to evaluate the cytoprotective effects in the same conditions of glucose toxicity.

To clarify the cytoprotective effect of GLP-1R signaling *in vivo*, we used a murine isogenic islet transplantation model using a suboptimal number of islets together with exendin-4 treatment, a degradation-resistant GLP-1 analog [12]. As isogenic islet grafts in the natural course of the early posttransplant period are easily lost due to various physiological stress [13], various suboptimal number of islet transplantation can lead proper engraftment during the transplantation process without regard for the effects of improved blood glucose levels following transplantation

* Corresponding author. Address: Department of Diabetes and Clinical Nutrition, Graduate School of Medicine, Kyoto University, 54 Kawahara-cho, Shogoin Sakyo-ku, Kyoto 606-8507, Japan. Fax: +81 75 751 4244.
E-mail address: inagaki@metab.kuhp.kyoto-u.ac.jp (N. Inagaki).

0006-291X/$ - see front matter © 2008 Elsevier Inc. All rights reserved.
doi:10.1016/j.bbrc.2008.01.046

of an optimal number of islets. When a higher suboptimal mass of islets is transplanted, blood glucose levels remain high during the early posttransplant period, changing to normoglycemic only during the late posttransplantation period if the engrafted mass is sufficient but remaining in the hyperglycemic state if the engrafted mass is insufficient. Thus, when a suboptimal number of islets are transplanted together with exendin-4 treatment in the early posttransplant period when the recipient is hyperglycemic, its indirect action on glucose tolerance can be excluded and its cytoprotective effect can be evaluated by monitoring the blood glucose levels. In addition, bio-imaging technology permits comparison of the number and mass of islets before and after transplantation.

In the present study, we evaluated the cytoprotective effect of GLP-1R signaling *in vivo* in pancreatic beta cells using a murine isogenic islet transplantation model. We used a suboptimal mass of transplanted islets with and without exendin-4 treatment, and monitored blood glucose levels. We also compared the number and mass of islet grafts with and without exendin-4 treatment under conditions of hyperglycemia.

Materials and methods

Animal care. All experiments were approved by the Kyoto University Animal Care Committee.

Animals. Male C57BL/6JJcl mice (CREA, Japan) aged 8–10 weeks were used as recipients and donors. Male transgenic C57BL/6-EGFP mice aged 8–10 weeks were also used as donors. The mice were obtained from Dr. Masaru Okabe (Research Institute for Microbial Diseases, Osaka University, Osaka, Japan) [14]. Recipient animals were rendered diabetic by a single intraperitoneal injection of streptozotocin (Sigma–Aldrich, USA), 120 mg/kg body weight, freshly dissolved in 10 mM citrate buffer (pH 4.2). Mice with a blood glucose concentration greater than 20 mmol/l for 2 consecutive days were used as recipients. Blood glucose concentrations were determined by glucose meter (Glucocard, Arkley, Japan).

Islet isolation, islet transplantation, and exendin-4 treatment. Islets were isolated, as previously described [15]. Recipient mice were anesthetized by isoflurane (Forane, Abott, Japan). Fresh islets in a volume of 400 μl PBS solution were injected into the portal vein and transplanted into the right hepatic lobe as previously described [15,16]. Exendin-4 at a dosage of 1.0 nmol/kg body weight was administered intraperitoneally once daily in the morning for 14 days.

Oral glucose tolerance test (OGTT). After fasting for 16 h, a basal blood sample was collected and the mice received glucose (1.5 g/kg body weight) orally; additional blood samples were collected at 15, 30, 60, 90, and 120 min after glucose loading.

Evaluation of number and mass of EGFP-expressing islet grafts. Islets isolated from transgenic C57BL/6-EGFP mice were first observed by fluorescence microscope BZ-8000 (KeyEnce, Japan) before transplantation; the area of fluorescence was measured using Image J software (National Institute of Mental Health, USA). Livers bearing islet grafts were removed and sectioned into 500-μm slices and serialized; digitalized photographs of all sections were taken. The number of EGFP-positive islets in each liver section was then counted, excepting those appearing by their position to be part of an islet in an adjacent section. The total area of fluorescence of all islets was then measured.

Measurement of beta-cell mass using immunohistochemistry. The right hepatic lobes were fixed, embedded in paraffin, cut in blocks at regular intervals, and sectioned into 5-μm sections. Deparaffinized sections were incubated with a polyclonal guinea pig anti-insulin antibody (Dako, USA), then with a biotinylated goat anti-guinea pig antibody (Vector, USA), and then with a streptavidin peroxidase conjugate and substrate kit (Dako). The total liver area and total insulin-positive beta-cell area were quantified using Image J software.

Apoptosis detection. TUNEL staining was performed using Apoptosis detection Kit (Takara Bio, Japan).

Statistical analyses. All data are presented as means ± SEM. Statistical analyses were performed by an unpaired *t*-test. p value of less than 0.05 was considered significant.

Results

Exendin-4 decreased the number of islet grafts required to restore normoglycemia

To evaluate the cytoprotective effect of GLP-1R signaling during the early posttransplant phase, we performed isogenic islet transplantation and observed blood glucose levels during the late posttransplant phase. Previous reports have shown that transplantation of only 75 islets can normalize blood glucose levels if the majority becomes engrafted [17], but because many islets are lost due to various stress such as glucotoxicity, transplantation of 75 islets is insufficient for restoration of normoglycemia. In our preliminary experiments, while some recipients showed improved blood glucose levels when 200 islets were transplanted (data not shown), no recipients showed any change in blood glucose levels when 150 islets were transplanted (Fig. 1A). Thus, 150 islets was chosen as an appropriate suboptimal number for use in these transplantation experiments. In addition, all mice transplanted with 150 islets together with exendin-4 treatment became hyperglycemic soon after transplantation but became normoglycemic approximately 14 days after transplantation (Fig. 1A). The responsibility of the islet grafts in exendin-4-treated mice in maintenance of glucose tolerance is demonstrated by the immediate return to hyperglycemia after removal the right hepatic lobe (Fig. 1B). In addition, OGTT was similar in mice receiving 150 islets with exendin-4 treatment and sham-operated control mice (Fig. 1C). These results indicate that exendin-4 treatment played a crucial role in the restoration of normoglycemia by protecting the transplanted islets from damage during the early posttransplant phase.

Detection of fluorescence of transplanted Islets of transgenic C57BL/6-EGFP mice

To clarify the cytoprotective effect of exendin-4 *in vivo*, we established a novel system whereby the total number and the total mass of islets can be compared before and after transplantation by using fluorescent islets isolated from transgenic C57BL/6-EGFP mice. These mice exhibited normal pancreas and islet morphology and well as normal glucose tolerance by OGTT (data not shown).

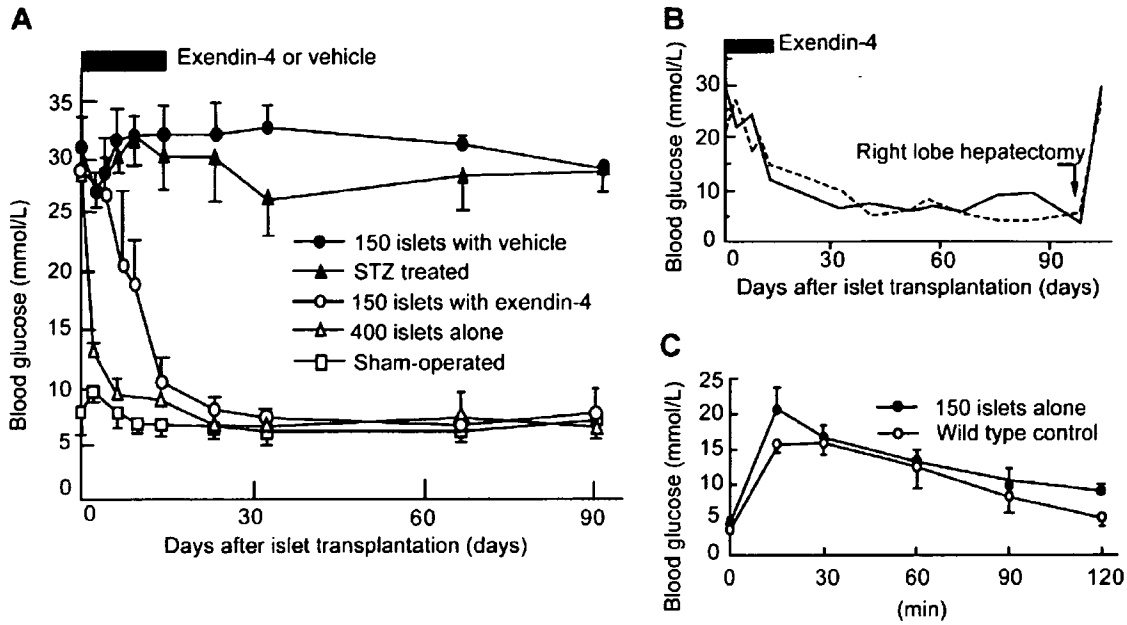

Fig. 1. Exendin-4 reduced the number of islets required for transplantation to restore normoglycemia in STZ-induced diabetic mice. (A) Blood glucose concentrations were measured in mice transplanted with 150 islets together with 1 nmol/kg exendin-4 treatment (open circles, $n = 4$), 400 islets alone (filled triangles, $n = 5$), 150 islets alone (filled circles, $n = 3$), STZ-treated only (filled triangles, $n = 5$), and Sham-operated C57BL/6 mice (open squares, $n = 5$). (B) Right hepatic lobe was resected from two recipients transplanted with 150 islets together with exendin-4 treatment on Day 90 to clarify the effect of the islet grafts on glycemic control. (C) OGTT was performed on Day 30 in recipients transplanted with 150 islets together with exendin-4 treatment and in sham-operated wild-type C57BL/6 mice ($n = 3$ for each).

Transplanted islets of transgenic C57BL/6-EGFP mice are traceable and measurable in both number and mass

To confirm traceability and measurability of the transplanted islets, intraportal transplantation of islets isolated from transgenic C57BL/6-EGFP mice was performed. One day and three days after transplantation, the right hepatic lobe was resected and sliced, and each slice was photographed by fluorescence microscope (Fig. 2A–C). Liver slices containing islet grafts were then immunostained for insulin. The area of fluorescence (Fig. 2A) coincided with that of the islet beta cells stained for insulin (Fig. 2B), demonstrating traceability of the islets. The number of islet grafts in the liver after transplantation was then compared. When 25, 50, or 75 islets were transplanted, the total number of islet grafts detected in the liver was 24.3 ± 0.3, 48.7 ± 0.8 and 73.3 ± 0.3, respectively ($n = 3$ for each), demonstrating a significant ($p < 0.0001$), strong correlation ($r = 1.000$) between the number of detected islet grafts in the liver and the number of transplanted islets (Fig. 2E). In addition, because the area of fluorescence coincided with that of immunostained islets (Fig. 2A–C), the total area of fluorescence reflected the total area mass of the islets, allowing comparison of total islet mass before and after transplantation. When 25, 50, and 75 islets were transplanted, the total area mass of islets before transplantation was 2.01 ± 0.04, 4.11 ± 0.01, and 5.89 ± 0.09 (mm^2), respectively, while that of islet grafts in the liver were 2.00 ± 0.02, 4.28 ± 0.07, and 6.08 ± 0.03 (mm^2), respectively ($n = 3$ for each), demonstrating a significant ($p < 0.0001$), strong ($r = 0.998$) correlation between before and after transplantation (Fig. 2F).

Exendin-4 reduced loss of transplanted islets from transgenic C57BL/6-EGFP mice during the early posttransplant phase

To exclude the indirect effect of exendin-4 through its effect on blood glucose levels, we reduced the number of the transplanted islets to 50. When 50 islets of transgenic C57BL/6-EGFP mice were transplanted with or without treatment of exendin-4 into STZ-induced diabetic mice, the blood glucose levels were not significantly different on 1 day (Day 1) ($n = 3$, 27.1 ± 0.3 vs 27.8 ± 0.1 (mmol/l), $p = 0.193$) or 3 days (Day 3) after transplantation ($n = 3$, 28.7 ± 0.2 vs 28.7 ± 0.3 (mmol/l), $p = 0.936$). The number and the total area mass of the islet grafts in livers resected on Day 1 (figure not shown) and Day 3 (Fig. 3A and B) were then examined. The number of islet grafts with treatment of exendin-4 (Ex(+)) showed 9.4% and 19.9% increases on Day 1 ($n = 3$ for each, 46.7 ± 0.51 vs 42.0 ± 0.33, $p < 0.05$) and Day 3 ($n = 3$ for each, 44.6 ± 0.36 vs 34.7 ± 0.84, $p < 0.01$) (Fig. 3C) compared to those without treatment (Ex(−)). Ex(+) islet grafts exhibited 29.0% and 31.9% more total area mass on Day 1 ($n = 3$ for each, $69.5 \pm 2.5\%$ vs $53.3 \pm 2.1\%$ (normalized to the total fluorescence area mass before transplantation), $p < 0.05$) and Day 3 ($n = 3$ for each, $64.5 \pm 2.6\%$ vs $26.9 \pm 1.1\%$, $p < 0.05$) (Fig. 3D), respectively, than Ex(−).

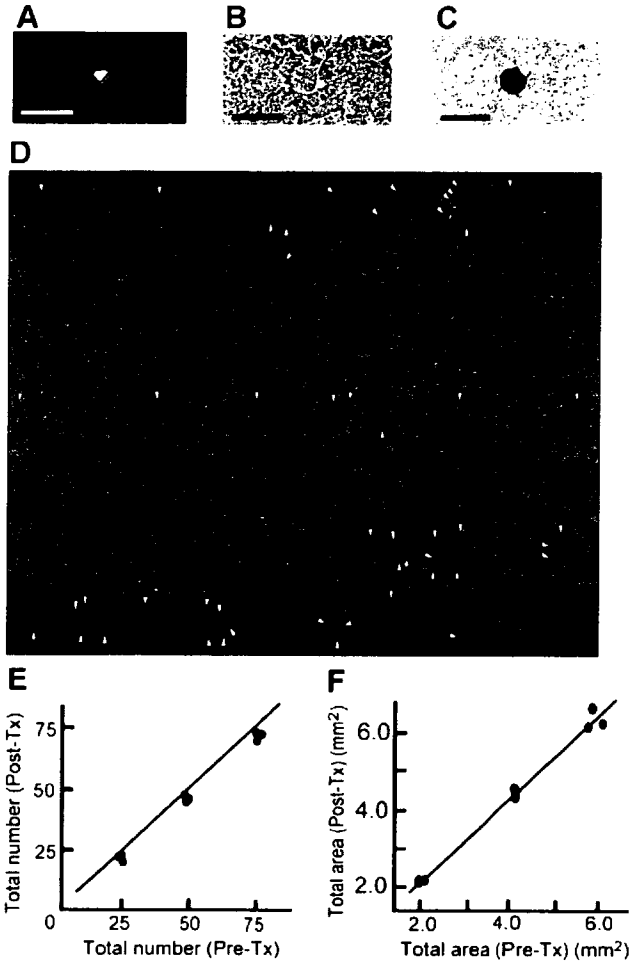

Fig. 2. Islets of transgenic C57BL/6-EGFP mice detected and measured by fluorescence microscopy. (A–C) Photographs of islet grafts in liver. Fluorescent islet (A), HE (B) and insulin immunostaining (C). Scale bar: 200 μm. (D) Representative photographs after transplantation with 50 islets of liver slices under fluorescence microscope. Fluorescent islets are indicated by arrowhead. (E, F) The total number (E) and the total area mass (F) of all EGFP-expressing islets before transplantation compared with fluorescent islet grafts in liver after transplantation ($n = 3$).

Area of islet grafts in liver with and without exendin-4 treatment compared by conventional immunohistochemical analysis

Conventional total area mass measurements, the ratio of the area of islet beta cells to that of the examined liver slice, was compared by immunohistochemical analysis using limited liver sections on Day 1 and Day 3 (Fig. 4A(a and c) and B (e and g)). The conventional relative area mass in Ex(+) was 32.0% and 44.7% higher on Day 1 ($n = 3$ for each, $0.07830 \pm 0.0003\%$ vs $0.0533 \pm 0.0003\%$, $p < 0.05$) and Day 3 ($n = 3$ for each, $0.0680 \pm 0.0009\%$ vs $0.0380 \pm 0.0043\%$, $p < 0.01$) than Ex(−) (Fig. 4C). The ratio of conventional relative area mass of Ex(+) to that of Ex(−) on Day 1 and Day 3 was comparable to the results of measurement of total area mass measured by our novel method.

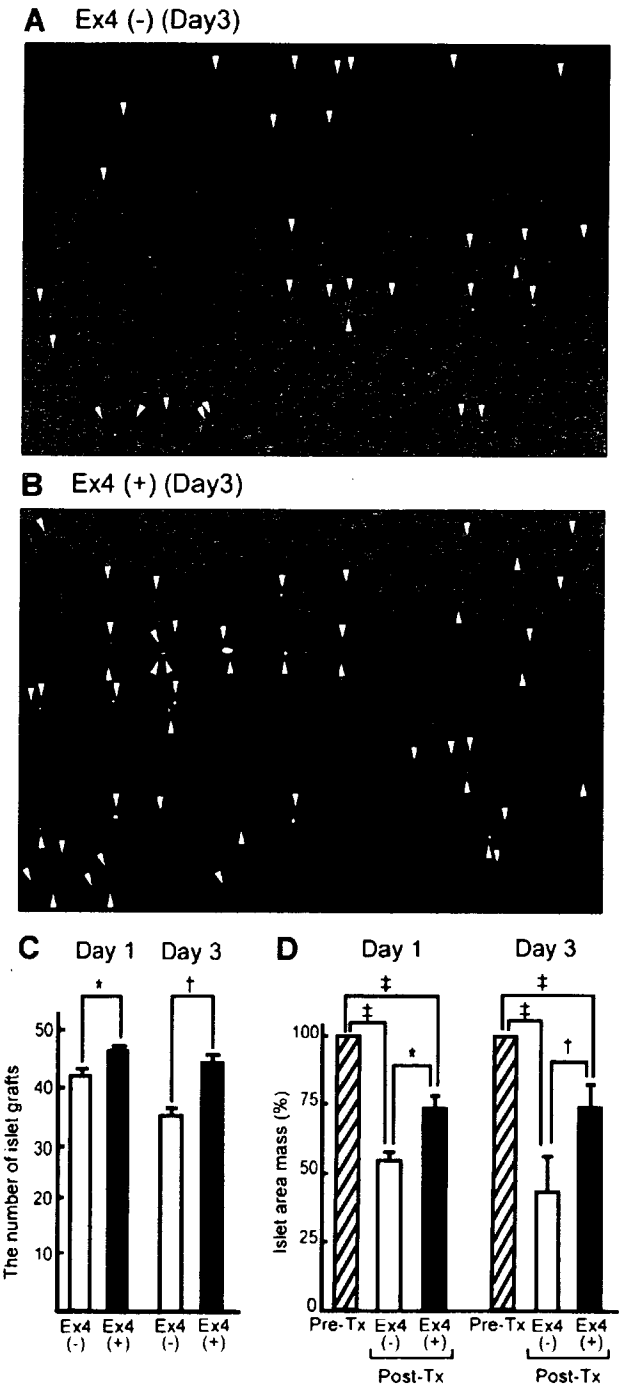

Fig. 3. Exendin-4 preserved transplanted islets during the early posttransplant period in number and total area mass. (A–B) Representative photographs of fluorescent islet grafts in all liver slices from exendin-4-treated mice (Ex4(+)) (A) and -untreated mice (Ex4(−)) (B) on Day 3. (C) Number of islet grafts in liver slices on Day 1 ($n = 3$) and Day 3 ($n = 3$) in Ex4(+) and Ex4(−). $^{*}p < 0.05$ and $^{\dagger}p < 0.01$ vs Ex4(−). (D) Total area mass of all fluorescent islet grafts in liver slices on Day 1 ($n = 3$) and on Day 3 ($n = 3$) in Ex4(+) and Ex(−). Data after transplantation (Post-Tx) and before transplantation (Pre-Tx) are also compared. $^{*}p < 0.05$ and $^{\dagger}p < 0.01$ vs Ex4(−). $^{\ddagger}p < 0.01$ vs Pre-Tx.

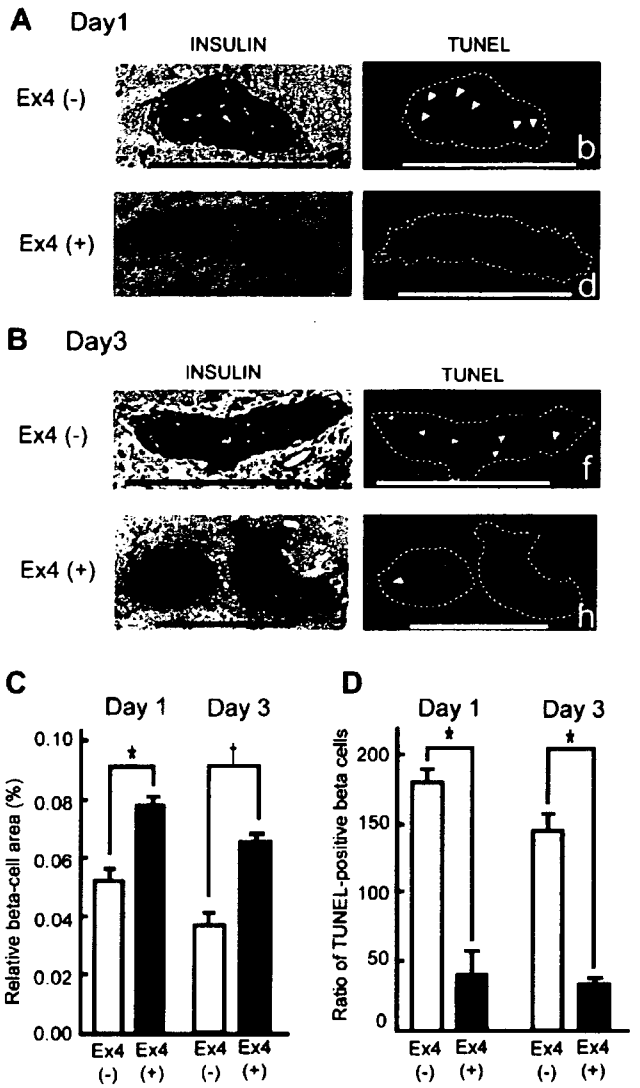

Fig. 4. Exendin-4 treatment reduced beta-cell apoptosis after intraportal islet transplantation. (A–B) Representative photographs of liver sections on Day 1 (A) and Day 3 (B) from Ex4(+) mice and Ex4(−) mice stained for insulin (a, c, e, and g) and TUNEL-assay (b, d, f, and h) are shown. TUNEL-positive cells are indicated by arrowhead. Scale bar: 200 μm. (C) Ex4(+) showed significantly greater beta-cell mass than Ex4(−) on Day 1 ($n = 3$ for each) and Day 3 ($n = 3$ for each). $^{*}p < 0.05$ and $^{\dagger}p < 0.01$ vs Ex4(−). (D) Ex4(+) showed a significantly greater decrease in the ratio of TUNEL-positive beta cells than Ex4(−) on Day 1 ($n = 3$ for each) (number/beta-cell area (mm^2)) and Day 3 ($n = 3$ for each) (number/beta-cell area (mm^2)). $^{*}p < 0.05$ vs Ex4(−).

Exendin-4 decreased the rate of apoptosis of beta cells introduced by intraportal islet graft after transplantation

To investigate the difference in area mass of transplanted islets in Ex(+) and Ex(−), the rate of apoptosis of beta cells of islet grafts on Day 1 and Day 3 was examined (Fig. 4A and B). The rate of apoptosis of TUNEL and insulin-double positive cells was significantly lower on Day 1 ($n = 3$ for each, 246.5 ± 5.5 vs 36.4 ± 3.6 (number/beta-cell area (mm^2), $p < 0.01$) and on Day 3 ($n = 3$ for each, 148.7 ± 17.7 vs 41.3 ± 1.3 (number/beta-cell area (mm^2), $p < 0.01$) with Ex(+) than Ex(−) (Fig. 4D).

Discussion

In the present study, we demonstrate that GLP-1R signaling has a cytoprotective effect in the posttransplant period using a murine islet transplantation model. Exendin-4 treatment during the early posttransplant hyperglycemic phase contributed to restore normoglycemia during the late posttransplant phase in STZ-induced diabetic mice receiving a suboptimal graft of 150 islets. In addition, the total number and total area mass of the islet grafts both on Day 1 and Day 3 was significantly greater in Ex(+) than in Ex(−). The finding that the rate of apoptosis was less in Ex(+) than in Ex(−) both on Day 1 and Day 3, when their blood glucose levels were yet unchanged, demonstrates that GLP-1R signaling inhibits apoptosis *in vivo* under conditions of glucose toxicity.

Murine islet transplantation is an ideal model for investigating the cytoprotective effect of exendin-4 on transplanted pancreatic beta cells *in vivo*. Although isogenic islets injected into the portal vein are spared rejection by the immune reaction, the cells may succumb to apoptosis due to various stress factors including hypoxia [18,19], inflammation [20,21], and mechanical shear stress [22,21] before engraftment. The efficacy of exendin-4 treatment on posttransplant hyperglycemic status in this transplantation model can be quantified using different suboptimal numbers of islets because the posttransplant glycemic condition directly reflects the mass of engrafted islets. The number and mass of transplanted islets can be traced because isolated islets can be labeled and examined before transplantation. Thus, this murine islet transplantation model allows observation of the direct effect of the cytoprotective effect on beta cells *in vivo*.

In this study, we established a method for tracing the transplanted islets of transgenic C57BL/6-EGFP mice in liver sections under fluorescence excitation. Our findings reveal that the area of fluorescence of islet grafts in liver coincides with that of insulin immunostaining (Fig. 2A–C), which areas before transplantation correlate highly with those after transplantation (Fig. 2F). Observation of each islet grafts before and after transplantation is definitive for evaluation of the cytoprotective action, which is not practicable by the conventional immunohistochemical method due to the necessarily limited observation of the organ.

We have also shown that the natural course of islet engraftment in the early posttransplant period can involve loss of about half of the transplanted beta cells. Recently, Eich et al. reported evaluation of islet mass by positron-emission tomography using islets labeled with ^{18}Fluorodeoxyglucose, and found that almost 50% of the transplanted islets in the graft were lost [23], which is comparable with our data. Although about 30% of the graft was found to be lost even with exendin-4 treatment on Day 1, the rate

of apoptosis remained lower, resulting in a mass of engraftment more than adequate for normoglycemia thereafter. This finding is encouraging regarding the possible clinical use of exendin-4 in islet transplantation therapy in human subjects [24,25].

Although exendin-4 is already in clinical use for treatment of T2DM [26], this cytoprotective effect on beta cells *in vivo* also certainly functions independently of other actions in T2DM. The mass of islets is usually already decreased when patients are diagnosed with T2DM [27]. Thus, exendin-4 treatment used in the early phase of development, when glycemic tolerance is yet normal, might hamper the progression of T2DM.

Acknowledgments

This work was supported in part by a Scientific Grant and a Grant-in-Aid for Exploratory Research from the Ministry of Education, Culture, Sports, Science, and Technology of Japan, and by Research on Nanotechnical Medicine from the Ministry of Health, Labour, and Welfare of Japan. We thank Dr. M. Okabe for providing us transgenic C57BL/6-EGFP mice.

References

[1] H. Elrick, L. Stimmler, C.J. Hlad Jr., Y. Arai, Plasma insulin response to oral and intravenous glucose administration, J. Clin. Endocrinol. Metab. 24 (1964) 1076–1082.

[2] M.J. Perley, D.M. Kipnis, Plasma insulin responses to oral and intravenous glucose: studies in normal and diabetic subjects, J. Clin. Invest. 46 (1967) 1954–1962.

[3] Y. Li, T. Hansotia, B. Yusta, F. Ris, P.A. Halban, D.J. Drucker, Glucagon-like peptide-1 receptor signaling modulates beta cell apoptosis, J. Biol. Chem. 278 (2003) 471–478.

[4] P.L. Brubaker, D.J. Drucker, Minireview: Glucagon-like peptides regulate cell proliferation and apoptosis in the pancreas, gut, and central nervous system, Endocrinology 145 (2004) 2653–2659.

[5] J.F. List, J.F. Habener, Glucagon-like peptide 1 agonists and the development and growth of pancreatic beta-cells, Am. J. Physiol. Endocrinol. Metab. 286 (2004) E875–E881.

[6] D.J. Drucker, The biology of incretin hormones, Cell Metab. 3 (2006) 153–165.

[7] B. Yusta, L.L. Baggio, J.L. Estall, J.A. Koehler, D.P. Holland, H. Li, D. Pipeleers, Z. Ling, D.J. Drucker, GLP-1 receptor activation improves beta cell function and survival following induction of endoplasmic reticulum stress, Cell Metab. 4 (2006) 391–406.

[8] J. Sun, H. He, B.J. Xie, Novel antioxidant peptides from fermented mushroom Ganoderma lucidum, J. Agric. Food Chem. 52 (2004) 6646–6652.

[9] H. Wang, G. Kouri, C.B. Wollheim, ER stress and SREBP-1 activation are implicated in beta-cell glucolipotoxicity, J. Cell Sci. 118 (2005) 3905–3915.

[10] L.A. Scrocchi, T.J. Brown, N. MaClusky, P.L. Brubaker, A.B. Auerbach, A.L. Joyner, D.J. Drucker, Glucose intolerance but normal satiety in mice with a null mutation in the glucagon-like peptide 1 receptor gene, Nat. Med. 2 (1996) 1254–1258.

[11] A.A. Young, B.R. Gedulin, S. Bhavsar, N. Bodkin, C. Jodka, B. Hansen, M. Denaro, Glucose-lowering and insulin-sensitizing actions of exendin-4: studies in obese diabetic (ob/ob, db/db) mice, diabetic fatty Zucker rats, and diabetic rhesus monkeys (*Macaca mulatta*), Diabetes 48 (1999) 1026–1034.

[12] L. Hansen, C.F. Deacon, C. Orskov, J.J. Holst, Glucagon-like peptide-1-(7–36)amide is transformed to glucagon-like peptide-1-(9–36)amide by dipeptidyl peptidase IV in the capillaries supplying the L cells of the porcine intestine, Endocrinology 140 (1999) 5356–5363.

[13] J.A. Emamaullee, A.M. Shapiro, Factors influencing the loss of beta-cell mass in islet transplantation, Cell Transplant. 16 (2007) 1–8.

[14] M. Okabe, M. Ikawa, K. Kominami, T. Nakanishi, Y. Nishimune, 'Green mice' as a source of ubiquitous green cells, FEBS Lett. 407 (1997) 313–319.

[15] T. Okitsu, S.T. Bartlett, G.A. Hadley, C.B. Drachenberg, A.C. Farney, Recurrent autoimmunity accelerates destruction of minor and major histoincompatible islet grafts in nonobese diabetic (NOD) mice, Am. J. Transplant. 1 (2001) 138–145.

[16] Y. Yonekawa, T. Okitsu, K. Wake, Y. Iwanaga, H. Noguchi, H. Nagata, X. Liu, N. Kobayashi, S. Matsumoto, A new mouse model for intraportal islet transplantation with limited hepatic lobe as a graft site, Transplantation 82 (2006) 712–715.

[17] A. King, J. Lock, G. Xu, S. Bonner-Weir, G.C. Weir, Islet transplantation outcomes in mice are better with fresh islets and exendin-4 treatment, Diabetologia 48 (2005) 2074–2079.

[18] G. Miao, R.P. Ostrowski, J. Mace, J. Hough, A. Hopper, R. Peverini, R. Chinnock, J. Zhang, E. Hathout, Dynamic production of hypoxia-inducible factor-1alpha in early transplanted islets, Am. J. Transplant. 6 (2006) 2636–2643.

[19] M. Giuliani, W. Moritz, E. Bodmer, D. Dindo, P. Kugelmeier, R. Lehmann, M. Gassmann, P. Groscurth, M. Weber, Central necrosis in isolated hypoxic human pancreatic islets: evidence for postisolation ischemia, Cell Transplant. 14 (2005) 67–76.

[20] N.R. Barshes, S. Wyllie, J.A. Goss, Inflammation-mediated dysfunction and apoptosis in pancreatic islet transplantation: implications for intrahepatic grafts, J. Leukoc. Biol. 77 (2005) 587–597.

[21] S. Cabric, J. Sanchez, T. Lundgren, A. Foss, M. Felldin, R. Kallen, K. Salmela, A. Tibell, G. Tufveson, R. Larsson, O. Korsgren, B. Nilsson, Islet surface heparinization prevents the instant blood-mediated inflammatory reaction in islet transplantation, Diabetes 56 (2007) 2008–2015.

[22] J.L. Contreras, C. Eckstein, C.A. Smyth, G. Bilbao, M. Vilatoba, S.E. Ringland, C. Young, J.A. Thompson, J.A. Fernandez, J.H. Griffin, D.E. Eckhoff, Activated protein C preserves functional islet mass after intraportal transplantation: a novel link between endothelial cell activation, thrombosis, inflammation, and islet cell death, Diabetes 53 (2004) 2804–2814.

[23] T. Eich, O. Eriksson, T. Lundgren, Visualization of early engraftment in clinical islet transplantation by positron-emission tomography, N. Engl. J. Med. 356 (2007) 2754–2755.

[24] E.A. Ryan, B.W. Paty, P.A. Senior, D. Bigam, E. Alfadhli, N.M. Kneteman, J.R. Lakey, A.M. Shapiro, Five-year follow-up after clinical islet transplantation, Diabetes 54 (2005) 2060–2069.

[25] K.A. Ghofaili, M. Fung, Z. Ao, M. Meloche, R.J. Shapiro, G.L. Warnock, D. Elahi, G.S. Meneilly, D.M. Thompson, Effect of exenatide on beta cell function after islet transplantation in type 1 diabetes, Transplantation 83 (2007) 24–28.

[26] D.M. Kendall, M.C. Riddle, J. Rosenstock, D. Zhuang, D.D. Kim, M.S. Fineman, A.D. Baron, Effects of exenatide (exendin-4) on glycemic control over 30 weeks in patients with type 2 diabetes treated with metformin and a sulfonylurea, Diabetes Care 28 (2005) 1083–1091.

[27] A.E. Butler, J. Janson, S. Bonner-Weir, R. Ritzel, R.A. Rizza, P.C. Butler, Beta-cell deficit and increased beta-cell apoptosis in humans with type 2 diabetes, Diabetes 52 (2003) 102–110.

0013-7227/08/$15.00/0
Printed in U.S.A.

Endocrinology 149(2):574–579

doi: 10.1210/en.2007-1292

The Murine Glucagon-Like Peptide-1 Receptor Is Essential for Control of Bone Resorption

Chizumi Yamada, Yuichiro Yamada, Katsushi Tsukiyama, Kotaro Yamada, Nobuyuki Udagawa, Naoyuki Takahashi, Kiyoshi Tanaka, Daniel J. Drucker, Yutaka Seino, and Nobuya Inagaki

Department of Diabetes and Clinical Nutrition (C.Y., Y.Y., K.T., K.Y., Y.S., N.I.), Kyoto University Graduate School of Medicine, and Core Research for Evolutional Science and Technology of Japan Science and Technology Cooperation (N.I), Kyoto 606-8507, Japan; Department of Internal Medicine (Y.Y.), Division of Endocrinology, Diabetes and Geriatric Medicine, Akita University School of Medicine, Akita 010-8543, Japan; Department of Biochemistry (N.U.) and Institute for Oral Science (N.T.), Matsumoto Dental University, Nagano 399-0781, Japan; Department of Nutrition (K.T.), Kyoto Women's University, Kyoto 605-8501, Japan; The Samuel Lunenfeld Research Institute (D.J.D.), Department of Medicine, Mount Sinai Hospital and the Banting and Best Diabetes Center, University of Toronto, Toronto, Canada M5G 2C4; Kansai Electric Power Hospital (Y.S.), Osaka 553-0003, Japan

Gastrointestinal hormones including gastric inhibitory polypeptide (GIP), glucagon-like peptide (GLP)-1, and GLP-2 are secreted immediately after meal ingestion, and GIP and GLP-2 have been shown to regulate bone turnover. We hypothesize that endogenous GLP-1 may also be important for control of skeletal homeostasis. We investigated the role of GLP-1 in the regulation of bone metabolism using GLP-1 receptor knockout (Glp-1r$^{-/-}$) mice. A combination of bone density and histomorphometry, osteoclast activation studies, biochemical analysis of calcium and PTH, and RNA analysis was used to characterize bone and mineral homeostasis in Glp-1r$^{-/-}$ and Glp-1r$^{+/+}$ littermate controls. Glp-1r$^{-/-}$ mice have cortical osteopenia and bone fragility by bone densitometry as well as increased osteoclastic numbers and bone resorption activity by bone histomorphometry. Although GLP-1 had no direct effect on osteoclasts and osteoblasts, Glp-1r$^{-/-}$ mice exhibited higher levels of urinary deoxypyridinoline, a marker of bone resorption, and reduced levels of calcitonin mRNA transcripts in the thyroid. Moreover, calcitonin treatment effectively suppressed urinary levels of deoxypyridinoline in Glp-1r$^{-/-}$, mice and the GLP-1 receptor agonist exendin-4 increased calcitonin gene expression in the thyroid of wild-type mice. These findings establish an essential role for endogenous GLP-1 receptor signaling in the control of bone resorption, likely through a calcitonin-dependent pathway. (*Endocrinology* 149: 574–579, 2008)

BONE IS CONTINUOUSLY remodeled throughout life, and osteoblastic bone formation and osteoclastic bone resorption are closely coordinated by a variety of local and systemic factors to maintain constant bone mass. Bone resorption is known to be rapidly inhibited by acute nutrient ingestion, suggesting that it might be mediated by other physiological factors, the levels of which change in response to the nutritional state such as incretins. Gastrointestinal hormones including gastric inhibitory polypeptide (GIP), glucagon-like peptide (GLP)-1, and GLP-2 are secreted immediately upon meal ingestion, although the fasting level of these peptides is low. GIP and GLP-2 are known to be involved in the regulation of bone turnover (1, 2).

The effect of GIP on bone has been extensively investigated *in vitro* and *in vivo*. The GIP receptor is expressed in osteoblasts (3), and GIP increases collagen type 1 expression and alkaline phosphatase activity in osteoblast-like cells (3) and protects osteoblasts from apoptosis (2), consistent with an anabolic effect. Recently, the presence of the GIP receptor in osteoclasts has been reported, and GIP has been shown to inhibit PTH-induced bone resorption, suggesting that a role of the postprandial rise in GIP is to stop active bone resorption such as occurs during fasting (4). The physiological importance of GIP receptor signaling on bone *in vivo* has been demonstrated using GIP receptor knockout (Gipr$^{-/-}$) mice, which exhibit a low bone mass phenotype due to both decreased bone formation and increased bone resorption (2, 5); and conversely, GIP-overexpressing transgenic mice exhibit increased bone mass (6).

GLP-2 is cosecreted with GLP-1 from L cells in the small and large intestine, and acts in the intestine to stimulate mucosal growth and nutrient absorption. Acute administration of GLP-2 decreases serum and urine markers of bone resorption in postmenopausal women (1, 7, 8), whereas bone formation appears to be unaffected by treatment with exogenous GLP-2. The effect of GLP-2 on bone has been investigated predominantly in humans, and the mechanism(s) underlying the GLP-2-mediated modulation of bone turnover remain unclear.

GLP-1 is well known as an incretin, and meal-stimulated plasma levels of GLP-1 are known to be diminished in patients with impaired glucose tolerance or type 2 diabetes (9). GLP-1 also has effects independent of insulin secretion such as inhibition of glucagon secretion and gastric emptying. In

First Published Online November 26, 2007

Abbreviations: BMC, Bone mineral content; BMD, bone mineral density; BS, bone surface; BV, bone volume; CT, computed tomography; DPD, deoxypyridinoline; ES, eroded surface; GIP, gastric inhibitory polypeptide; GLP, glucagon-like peptide; N.Mu.Oc, number of multinuclear osteoclasts; N.Oc, number of osteoclasts; TV, tissue volume; WT, wild type.

Endocrinology is published monthly by The Endocrine Society (http://www.endo-society.org), the foremost professional society serving the endocrine community.

contrast to information derived from studies of GIP and GLP-2 on bone formation and resorption, the physiological role of GLP-1, if any, on bone is completely unknown. Because the GLP-1 receptor is expressed in thyroid C cells, and GLP-1 directly stimulates the secretion of calcitonin (10, 11), a potent inhibitor of osteoclastic bone resorption, GLP-1 may contribute to nutrient-mediated reduction of bone resorption.

In the present study, we have investigated the role of endogenous GLP-1 in the regulation of bone metabolism using GLP-1 receptor knockout (Glp-1r $^{-/-}$) mice. We performed morphological analyses of bones from Glp-1r$^{-/-}$ mice and wild-type (WT) littermate controls, including densitometry and histomorphometry. We also evaluated the effects of exogenous GLP-1 on thyroid C cells, and we determined the effect of calcitonin treatment in Glp-1r $^{-/-}$ mice. Taken together, our data illustrate an essential role for the GLP-1 receptor in the control of bone resorption.

Materials and Methods

Animals

Glp-1r$^{-/-}$ mice and Glp-1r$^{+/+}$ littermate WT controls were maintained on a C57BL/6 background as described previously (12). Mice were kept in cages with four to six animals per cage with free access to standard rodent diet and water. Male mice were used for all experiments. Crown to rump length was measured from tip of the nose to the end of the body. All procedures for animal care were approved by the Animal Care Committee of Kyoto University Graduate School of Medicine.

Bone densitometry and body composition analysis

For computed tomography (CT)-based analysis of bone mineral density (BMD), 10-wk-old WT and Glp-1r$^{-/-}$ mice were anesthetized with ip injections of pentobarbital sodium (Nembutal; Dainippon Pharmaceutical, Osaka, Japan). Tibiae (between proximal and distal epiphysis) and lumber spines (between L2 and L4) were scanned at 1-mm intervals using an experimental animal CT system (LaTheta LCT-100; Aloka, Tokyo, Japan). Bone mineral content (BMC) (milligrams), bone volume (cubic centimeters), and BMD (milligrams per cubic centimeter) were calculated using the LaTheta software (version 1.00). The minimum moment of inertia of cross-sectional areas (milligram-centimeters), which represents the flexural rigidity, and the polar moment of inertia of cross sectional areas (milligram-centimeters), which represents the torsional rigidity, were also calculated automatically by the LaTheta software (13). For body composition analysis, the whole bodies of 10-wk-old WT and Glp-1r$^{-/-}$ mice were scanned using the LaTheta CT system.

Bone histomorphometry

Six-week-old male mice were used for studies of bone histomorphometry as described previously (2). Briefly, mice were double labeled with sc injections of 30 mg/kg tetracycline hydrochloride (Sigma Chemical Co., St. Louis, MO) 4 d before being killed and 10 mg/kg calcein (Dojindo Co., Kumamoto, Japan) 2 d before being killed. Bones were stained with Villanueva bone stain for 7 d, dehydrated in graded concentrations of ethanol, and embedded in methyl-methacrylate (Wako Chemicals, Osaka, Japan) without decalcification. Bone histomorphometric measurements were made using a semiautomatic image analyzing system (System Supply, Ina, Japan) and a fluorescent microscope (Optiphot; Nikon, Tokyo, Japan) set at a magnification of ×400. Standard bone histomorphometrical nomenclatures, symbols, and units were used as described in the report of the American Society of Bone and Mineral Research Histomorphometry Nomenclature Committee (14).

Osteoclast and osteoblast assays

For osteoclast differentiation assay, mouse primary osteoblasts and bone marrow cells were cocultured for 7 d in α-MEM (Sigma) containing 10% fetal bovine serum in the presence or absence of 10^{-8} M 1α,25-dihydroxyvitamin D_3 with or without 10^{-5} M GLP-1 (Peptide Institute, Inc., Osaka, Japan). Cells positively stained for tartrate-resistant acid phosphatase containing more than three nuclei were counted as osteoclasts (15, 16). For pit formation assay of mature osteoclasts (16), aliquots of crude osteoclast preparations were plated on dentine slices and cultured with or without 10^{-4} M GLP-1 or 10^{-10} M calcitonin (Peptide Institute) for 48 h. The number of resorption pits was quantified under scanning electron microscopy. For osteoblast apoptosis assay, Saos-2 osteoblasts (Dainippon Pharmaceutical Co., Ltd., Osaka, Japan) were pretreated for 1 h with or without 10^{-6} M GLP-1 and then incubated for an additional 6 h in the presence or absence of 50 μM etoposide, as described previously (2).

Biochemical measurements

Total calcium concentration was measured using Spotchem SP-4420 (Arkray, Kyoto, Japan), and ionized calcium was measured using a blood gas analyzer (GEM premier 3000; Instrumentation Laboratory, Tokyo, Japan) after overnight fasting and 6 h after refeeding. Plasma insulin, leptin, and intact PTH levels were determined by ELISA kits for mouse insulin (Shibayagi, Gunma, Japan), mouse leptin (Morinaga, Yokohama, Japan) and mouse intact PTH (Immutopics Inc., San Clemente, CA). Urinary deoxypyridinoline (DPD) concentrations were measured using an ELISA kit (Quidel, San Diego, CA) before and at 4 h after single administration of 10 IU/kg eel calcitonin (Elcitonin; Asahi Kasei Pharma, Tokyo, Japan).

RNA preparation and quantitative real-time PCR

For analysis of thyroid calcitonin gene expression, mice were injected ip with the GLP-1 receptor agonist exendin-4 (Sigma) at a dose of 24 nmol/kg or the same volume of PBS 6 h before RNA isolation. Total RNA was extracted from thyroid tissue using RNeasy Mini Kit (QIAGEN, Valencia, CA). cDNAs were synthesized by SuperScript II Reverse Transcriptase system (Invitrogen, Carlsbad, CA) and subjected to quantitative real-time PCR using SYBR Green master kit and the ABI PRISM 7000 Sequence Detection System (Applied Biosystems, Foster City, CA). Primers for the calcitonin gene were calcitonin forward 5′-CTCACCAGGAAGGCATCAT-3′ and calcitonin reverse 5′-CAGCAGGCGAACTTCTTCTT-3′. The relative amount of mRNA was calculated with glyceraldehyde-3-phosphate dehydrogenase (GAPDH) mRNA as the invariant control: GAPDH forward 5′-TCGTTGATGGCAACAATCTC-3′ and GAPDH reverse 5′-AAATGGTGAAGGTCGGTGTG-3′.

Statistical analysis

Results are expressed as means ± SE. Statistical significance was assessed by ANOVA and unpaired Student's *t* test, where appropriate. A P value of <0.05 was considered to be statistically significant.

Results

Baseline characteristics of WT and Glp-1r$^{-/-}$ mice

Growth of Glp-1r$^{-/-}$ mice was similar to that of WT mice in body weight during the 50-wk observation period (supplemental Fig. 1A, published as supplemental data on The Endocrine Society's Journals Online web site at http://endo.endojournals.org). Body length and length of tibia measured at 10 and 50 wk of age were also almost identical to each other (supplemental Fig. 1, B and C). No significant difference was observed in fat mass (supplemental Fig. 1D) and lean body mass (supplemental Fig. 1E) between 10-wk-old WT and Glp-1r$^{-/-}$ mice determined by CT-based body composition analysis. Similarly, plasma leptin levels (supplemental Fig. 1F) were comparable in 10-wk-old WT and Glp-1r$^{-/-}$ mice. These data indicate that there was no difference between WT and Glp-1r$^{-/-}$ mice in body mass, body composition, or hormone levels that might affect bone mass.